BIOPHYSICAL STUDY OF THE ENDOPLASMIC RETICULUM MASTER REGULATOR PROTEIN, BIP, AS A MOLECULAR MOTOR

Tesis entregrada a

LA UNIVERSIDAD DE VALPARAÍSO

en cumplimiento Parcial de los requisitos para optar al grado de
Doctor en Ciencias con Mención en Biofísica y Biología Computacional

Facultad de Ciencias

por

Hilda Marta Alfaro Valdés

Agosto 2026

Dirigida por: **Dr. Christian A. M. Wilson**

FACULTAD DE CIENCIAS

UNIVERSIDAD DE VALPARAÍSO

INFORME DE APROBACIÓN
TESIS DE DOCTORADO

Se informa a la Facultad de Ciencias que la Tesis de Doctorado presentada por:

Hilda Marta Alfaro Valdés

Ha sido aprobada por la Comisión de Evaluación de la tesis como requisito para optar al grado de Doctor en Ciencias con mención en Biofísica y Biología Computacional, en el examen de Defensa de Tesis rendido el día 31 del mes de agosto de 2026.

Director de tesis:

Dr. Christian A. M. Wilson ----------

Comisión de Evaluación de la Tesis

Dr. David Naranjo ----------

Dr. Ramón Latorre ----------

Dr. Alan Neely ----------

Dedicada a mi Pablo, Elisa, mis padres Marta y José, junto a mis hermanos Sofía, Felipe y mi sobrino Tomás. A mis abuelos. Con todo mi Amor

Si tienen fe tan pequeña como un grano de mostaza,
le dirán a esta montaña: "Muévete de aquí para allá",
y se moverá.
Nada les será imposible
Mateo, 17:20

Agradecimientos

Llegar hasta aquí ha sido un camino largo, lleno de desafíos, aprendizajes, incertidumbres, descubrimientos y, sobre todo, de personas que hicieron posible llegar hasta el final. Estas palabras son para todos quienes, de una u otra forma, formaron parte de este proceso y dejaron una huella en mi vida.

A **Pablo**, mi compañero de vida, por caminar a mi lado durante este largo viaje. Por tu amor, tu paciencia, tu compañía y por estar presente en los días buenos y, especialmente, en aquellos en que el camino se hizo más difícil. Gracias por creer en mí, por acompañar mis sueños y por ser mi hogar en medio de tantos cambios.

A **Elisa**, mi niña, que llegó a mi vida de una manera que nunca imaginé y se convirtió en una parte tan importante de ella. Gracias por abrirme un espacio en tu corazón y por aceptarme como tu casi mami. Gracias por tus risas, tus abrazos, tus palabras fortalecedoras y por permitirme ser parte de tu vida.

A mi mamá **Marta Valdés**, a mi papá **José Alfaro** y a mis hermanos **Sofía** y **Felipe** junto a mi sobrino **Tomás**, por ser mis raíces y mi lugar de origen. Por su amor incondicional, por creer siempre en mí y por enseñarme, desde mucho antes de comenzar este camino, que con esfuerzo, perseverancia y valentía es posible alcanzar aquello que alguna vez parecía lejano.

A quienes ya no están, pero siguen viviendo en mi memoria y en mi corazón: mi abuelo **Pedro**, mi abuelita **Hilda**, mi padrino **Pedro** y **Robert Lesch**. En especial, a don **Bob**. No solo fue un gran científico, sino también un amigo científico, de esos que dejan una huella que trasciende los experimentos y los papers.

A **Christian Wilson**, mi tutor, quiero agradecerle haber sido mucho más que un tutor durante este camino. Gracias por tu confianza, por tu apoyo y por haber estado presente en uno de los momentos más difíciles de este proceso. Gracias por abrirme las puertas de tu laboratorio y recibirme cuando más lo necesitaba, por confiar en mi trabajo y por darme un espacio en el que pude continuar creciendo y desarrollándome como científica. Sobre todo, gracias por tu amistad. A **Cecilia D'Alessio**, quien fue como una cotutora para mí. Gracias por resolver mis dudas, por compartir tu conocimiento y por ser la gran mujer científica que eres; te admiro.

En segundo lugar, quiero agradecer profundamente al **Programa de Doctorado en Biofísica y Biología Computacional** por haber sido el espacio en el que pude crecer como científica y como persona. A **Patricio Orio**, quiero agradecerle especialmente por haberme ayudado a incorporarme a este programa tras un complejo proceso de cambio de programa. Gracias por haber confiado en mí; pude sentirme acogida y encontré un espacio en la ciencia. Mirando hacia atrás, sé que aquella oportunidad marcó un antes y un después en mi camino.

A mi comisión, **David Naranjo**, **Ramón Latorre** y **Alan Neely**, gracias por sus preguntas, sus comentarios y su exigencia científica. Cada uno de ustedes contribuyó de manera importante a mi formación, enseñándome a mirar la ciencia con el rigor que requiere, pero siempre desde un lugar profundamente humano. Me siento muy afortunada de haber tenido la oportunidad de aprender de excelentes científicos. A la directora del programa **Karen Castillo**, quien ayudó a finalizar este proceso. Me siento profundamente feliz y agradecida de haber formado parte de este programa.

A mis colegas y compañeros de laboratorio, gracias por compartir conmigo estos años de experimentos, preguntas, resultados, frustraciones, descubrimientos y aprendizajes. La ciencia puede ser un camino solitario muchas veces, pero ustedes hicieron que no lo fuera. Gracias por cada conversación, cada discusión científica, cada ayuda ante un experimento que no resultaba y cada momento compartido en el laboratorio.

A **Karina New**, **Camila Correa**, **Valentina Squicciarini**, **Andrea Avilés**, **Javiera**

Martínez, **don Luis**, **Sra. Yesica**, **Aaron** y **Flavia Livacic**, gracias por haber sido parte de este camino y por el apoyo que me brindaron en distintos momentos. A **Bernardo López**, un agradecimiento especialmente profundo por todo tu apoyo experimental y por tu enorme aporte a este trabajo y por tu generosidad. A **Pablo Galaz**, **Gicela Gutiérrez** y **Nicolás Cristi,** quienes me ayudaron a cerrar este trabajo.

A **Daniela Seelenfreund**, por haber sido un apoyo fundamental al comienzo de este proceso. Por haberme apoyado y acompañado en los momentos en que más lo necesitaba. A mi amiga **Liuba Peñate**, por acompañarme desde la amistad y por ser una fuente de fuerza durante todo el proceso. Especialmente, gracias por compartir generosamente conmigo y con mi familia esa sabiduría espiritual que tienes la bendición de tener.

A **Luka Robeson**, mi *roomie* de Valdivia, por compartir conmigo una etapa tan importante de mi vida y los inicios de mi PhD. Gracias por la compañía, las conversaciones, las risas. Como también a mis amigas de Valdivia, que me recibieron con tanta amabilidad sin siquiera conocerme, pero que, por esas cosas de la vida, teníamos mucho en común. **Paulina Fuentes** y su **mamá Sandra.**

A mis amigos Iquiqueños Gabo **(Gabriel Rojas)**, Fernandita **(María Fernanda Leal)**, la Fabi (**Fabiola Cruz)**, el Jose **(José Aguilera)**, la Caro **(María Carolina García)** y mi comadre **Denisse Miranda,** junto a mi ahijada **Mía,** como también a mis colegas de mi alma máter, **Universidad Arturo Prat**. **Karem Arriaza**, **Karen Flores** y **Eduardo Peña**. Por haber estado siempre presente, su aporte para mí ha sido esencial. Por haberme incluido en distintas actividades, charlas, cursos y clases que fueron fundamentales para mis postulaciones a la ANID. Gracias por ser tan colaborativos y por permitirme formar parte de Uds. a distancia.

A mis amigas santiaguinas, **Pilar Aleite y Romina Muñoz**, gracias por ser una parte importante de mi vida y por acompañarme en este camino. Gracias por recordarme, en medio de la ciencia y de las exigencias de este proceso, que también existía una vida fuera del laboratorio. También agradezco a quien fue una parte importante en el inicio de este proceso, **Natalie Casanova**. Por todo lo bueno que compartimos durante los años en que

nuestras vidas caminaron juntas. Al círculo más cercano a mí, a Pablo y a su familia, destacando a la **Abuelita Rosario**, quien me ha querido como su propia nieta desde el primer día que la conocí. A mis suegros, **Víctor Moya** y **Claudia Ponce**. A mis otros suegros, **Mané** y **Achim.** A los queridos amigos de Pablo, físicos de formación con sus respectivas parejas y/o esposas: **Simón**, **Alejandro**, **Macarena, Sebastián**, **Lucía**, **Víctor Pinto**, **Pauli, Roberto y Carolina**. Gracias por ser parte de este proceso y por compartir las alegrías, los logros y una palabra de aliento cuando más lo necesité.

A **Tamara Hermosilla** y **Diego Varela**, quienes fueron mis tutores durante el pregrado, gracias por seguir presentes y por continuar apoyándome cada vez que lo he necesitado.

A mi familia materna y paterna, en especial a **Claudia Cofre**, la pareja de mi papá, quien ha sido como una amiga para mí. Gracias, por tanto, por tus abrazos, tus palabras de aliento y de apoyo emocional en todo momento. Mi prima **Paulina**, a la **Marti,** su hija, a mi tía **Lila** y a **Nelson**. Como también a mi tía **Daysi**. Por todas las onces ricas a las que me invitaban mientras me preparaba para las entrevistas del PhD. A la **Sra. Pilar**, por ayudarme tanto en todo y, sobre todo, al final de este proceso. A todas aquellas personas que, aunque quizás no aparezcan mencionadas por nombre, formaron parte de este recorrido. A quienes me enseñaron algo, me ayudaron, me escucharon, me hicieron reír, compartieron conmigo una idea, un experimento, un café o simplemente un momento difícil. Cada uno dejó una pequeña huella en este camino.

Por último, agradecer especialmente y con cariño a la **ANID**. Por la mantención económica. Por orientarme durante mi cambio de programa. Profundamente agradecida a la institución que me permitió doctorarme. Gracias a mi Beca Nacional de doctorado del año 2022, N.º 21221149. También por la beca de pasantía y por los gastos operacionales, que contribuyeron a la culminación de mi tesis.

Un doctorado no se construye solo con resultados, publicaciones y experimentos. Se construye también con vínculos, confianza, paciencia, generosidad y compañía. A todos quienes hicieron de estos años no solo una etapa de formación científica, sino también una parte fundamental de mi historia, gracias.

Resumen

La translocación de proteínas hacia el retículo endoplásmico (RE) es un proceso celular fundamental, esencial para el correcto plegamiento, modificación y direccionamiento de las proteínas secretoras y de membrana. En eucariotas, este proceso ocurre mediante mecanismos cotraduccionales o postraduccionales; estos últimos son responsables de la translocación de proteínas al RE. A pesar de su importancia biológica, la vía postraduccional sigue siendo desconocida. El translocón Sec61 constituye el canal central por el que los polipéptidos atraviesan la membrana del RE.

La chaperona residente del RE, BiP (por sus siglas en inglés, immunoglobulin binding protein), miembro de la familia Hsp70, desempeña un papel clave en este proceso al interactuar tanto con el sustrato polipeptídico como con el complejo Sec62/Sec63 asociado a Sec61, utilizando la energía derivada de la hidrólisis de ATP para facilitar la translocación y el plegamiento en el lumen del RE. Sin embargo, el mecanismo mecanoquímico mediante el cual BiP opera durante este proceso sigue siendo objeto de debate. Se han propuesto dos modelos: un trinquete browniano (*Brownian ratchet*) pasivo, en el que BiP impide el retroceso del polipéptido sin generar una fuerza mecánica mayor que la del baño térmico; y un modelo activo de golpe de potencia (*power stroke*), en el que BiP convierte la energía química en trabajo mecánico para impulsar el sustrato a través del canal.

Un estudio reciente de molécula única demostró que la secuencia señal del precursor del factor alfa (ppαF) permanece asociada al complejo Sec61 durante aproximadamente 17 segundos, lo que sugiere una ventana temporal en la que BiP puede interactuar de manera productiva con el dominio J de Sec63. Aunque el papel

exacto del dominio J aún no está completamente definido, se ha propuesto que la interacción entre BiP y el dominio J de Sec63 reduce la especificidad de BiP para sus sustratos, lo que le permite unirse a regiones extendidas de la cadena polipeptídica. En contraste, BiP en solución reconoce preferentemente un motivo consenso definido, Hy(WX)HyXHyXHy, donde Hy representa un residuo aromático o hidrofóbico voluminoso, W corresponde a triptófano y X puede ser cualquier aminoácido. Mediante el análisis de la cinética de translocación, caracterizamos la función motora de BiP mediante ensayos de protección frente a la proteasa *in vitro* utilizando microsomas de *Saccharomyces cerevisiae* y proteínas quiméricas diseñadas que contienen todos los componentes necesarios para la translocación postraduccional.

Para ello, diseñamos constructos quiméricos compuestos por un péptido señal (reconocido por Sec61), una región desplegada (Dominio I27 mutante de Titina) que confiere competencia para la translocación y un dominio plegado correspondiente a una proteína de alta o baja fuerza de desplegamiento, previamente reportados en la literatura mediante pinzas ópticas (*optical tweezers*). En primer lugar, se utilizó como control positivo una proteína quimérica compuesta por dos dominios del dominio I27 mutante de Titina en el ensayo de protección frente a proteasas, la cual se translocó hacia los microsomas a una tasa de 0,61 %/min. Por el contrario, la proteína quimérica de Top7 (que requiere 20 pN para su desplegamiento) no mostró translocación detectable, mientras que la quimera de calmodulina, cuyo desplegamiento ocurre a 7 pN, exhibió una tasa de translocación de 0,03 %/min.

Esta baja eficiencia de translocación *in vitro* sugiere que BiP no ejerce fuerzas suficientes para desplegar las proteínas y permitir su translocación. Además, el trabajo mecánico estimado y la potencia de salida fueron comparables a la energía térmica local y de órdenes de magnitud menores que los de motores moleculares de

tipo activo (*power stroke*) bien caracterizados, respectivamente. En conjunto, sugerimos que estos resultados descartan un mecanismo en el que BiP genera un trabajo mecánico sustancial para traccionar y desplegar los sustratos en translocación y, en su lugar, respaldan un mecanismo de tipo trinquete (*ratchet*) para la translocación de proteínas mediada por BiP.

Abstract

Protein translocation to the endoplasmic reticulum (ER) is a fundamental cellular process, essential for the correct folding, modification, and targeting of secretory and membrane proteins. In eukaryotes, this process occurs through co-translational or post-translational mechanisms; the latter mediates protein translocation to the ER. Despite its biological importance, the post-translational pathway remains largely unknown. The Sec61 translocon constitutes the central channel through which polypeptides cross the ER membrane.

The ER resident chaperone, BiP (immunoglobulin-Binding Protein), a member of the Hsp70 family, plays a key role in this process by interacting with both the polypeptide substrate and the Sec62/Sec63 complex associated with Sec61, using energy derived from ATP hydrolysis to facilitate translocation and folding within the ER lumen. However, the mechanochemical mechanism by which BiP operates during this process remains debated. Two models have been proposed: a passive Brownian ratchet, in which BiP prevents the polypeptide from recoiling without generating a mechanical force greater than that of the heat bath; and an active powerstroke model, in which BiP converts chemical energy into mechanical work to propel the substrate through the channel. A recent single-molecule study demonstrated that the precursor alpha factor (ppαF) signal sequence remains associated with the Sec61 complex for approximately 17 seconds, suggesting a time window in which BiP can productively interact with the J domain of Sec63. Although the exact role of the J domain is not yet fully defined, it has been proposed that interaction between BiP and the J domain of Sec63 reduces BiP's substrate specificity, allowing it to bind extended regions of the polypeptide chain.

In contrast, BiP in solution preferentially recognizes a defined consensus motif, Hy(WX)HyXHyXHy, where Hy represents a bulky aromatic or hydrophobic residue, W corresponds to tryptophan, and X can be any amino acid. We characterized BiP motor function by analyzing translocation kinetics using *in vitro* protease protection assays with *Saccharomyces cerevisiae* microsomes and engineered chimeric proteins containing all components required for post-translational translocation.

To this end, we designed chimeric constructs composed of a signal peptide (recognized by Sec61), an unfolded region (mutant Titin I27 domain) that confers translocation competence, and a folded domain corresponding to a high- or low-unfolding-force protein, previously reported in the literature using optical tweezers. First, we used a chemical protein composed of two domains of the unfolded mutant Titin I27 domain as a positive control in the protease protection assay. This protein translocated into microsomes at a rate of 0.61%/min. In contrast, the Top7 chemical protein (which requires 20 pN for unfolding) showed no detectable translocation, while the calmodulin chimera, which unfolds at 7 pN, exhibited a translocation rate of 0.03%/min.

This low *in vitro* translocation efficiency suggests that BiP does not exert sufficient forces to unfold the proteins and allow their translocation. Furthermore, the estimated mechanical work and power output were comparable to the local thermal energy and orders of magnitude lower than those of well-characterized active molecular motors (powerstroke motors), respectively. Taken together, we suggest that these results rule out a mechanism in which BiP generates substantial mechanical work to pull and unfold substrates in translocation and instead support a ratchet-like mechanism for BiP-mediated protein translocation.

Publications during the thesis period

1. **Hilda M. Alfaro-Valdés***, Andrea Avilés, Valentina Squiacciarini, Aaron Paredes, Cecilia D´Alessio, Bernardo López, Javiera Martinez, Karina New, Christian A. M. Wilson, An Optimized and Scalable Protocol for Microsome Purification from Yeast for High-Resolution Biophysical Applications, in preparation.

2. **Hilda M. Alfaro-Valdés**, Karina New, Bernardo López, Pablo S. Moya, Francesca Burgos-Bravo, Carolina Ramírez-Álvarez, Pablo Galaz-Davison, Ariela Vergara-Jaque, Javiera Reyes, Robert Lesch, Cecilia D'Alessio, Randy Schekman, and Christian A.M. Wilson. The Endoplasmic Reticulum master regulator protein BiP acts as a ratchet molecular motor during protein translocation. Manuscript submitted to the Proceedings of the National Academy of Sciences (PNAS).

3. Christian A. M. Wilson, **Hilda M. Alfaro-Valdés, Merve Kaplan**, Cecilia D'Alessio, Mechanical effect of protein glycosylation on BiP-mediated post-translational translocation and folding in the endoplasmic reticulum, *Biophysical Reviews.* 2025; 17:435–447. doi:10.1007/s12551-025-01313-x.

4. Wendy N. Sánchez, Luka Robeson, **Hilda M. Alfaro-Valdés**, Katarzyna Tych, Ricardo A. Matute, Arnold J. M. Driessen, Christian A. M. Wilson*, Hydrophobicity and signal sequence binding to the Sec complex: A single-molecule biophysical perspective, *Biochemical and Biophysical Research Communications.* 2026; 832:154361. doi:10.1016/j.bbrc.2026.154361.

5. Luka Robeson, Nathalie Casanova-Morales, Francesca Burgos-Bravo, **Hilda M. Alfaro-Valdés**, Robert Lesch, Carolina Ramírez-Álvarez, Mauricio Valdivia-Delgado, Marcela Vega, Ricardo A. Matute, Randy Schekman, Christian A. M. Wilson*, Characterization of the interaction between the Sec61 translocon complex and ppαF using optical tweezers, *Protein Science.* 2024; 33:e4996. doi:10.1002/pro.4996.

List of Figures

Figure 1. Structure of the Sec complex by Cryo-EM. Below is a ribbon diagram of the Sec61 complex, obtained through cryo-electron microscopy of Saccharomyces cerevisiae.. 2

Figure 2. Scheme of the post-translational process of secretory protein in eukaryotic cells**.** 3

Figure 3. Mechanochemical mechanism of BiP function during post-translational translocation.. 5

Figure 4. Experimental model to investigate the mechanochemical mechanism of BiP in posttranslational translocation by protease protection assay 10

Figure 5. Generation of the yeast Sec63 (A179T) mutant. 12

Figure 6. Schematic of the development of an improved method for isolating yeast microsomes by combining the Parodi and Schekman methods 14

Figure 7. Schematic representation of the design of chimeric protein constructs. 17

Figure 8. Schematic representation of the Translocation and kinetics analysis by Western Blot. 23

Figure 9. Experimental optical tweezers setup for the unfolding of the chimeric Top 7 protein.. 29

Figure 10. Effect of temperature and presence of Ca^{+2} on the mechanical unfolding of the N-terminus of CaM through steered molecular dynamics (SMD) 31

Figure 11. Prepro-α-Factor (ppαF) translocation assay visualized by radioactivity and Western blotting 33

Figure 12. Translocation kinetics of chimera proteins. 35

Figure 13. Maximum translocation of chimeras at different temperatures and conditions. 37

Figure 14. Translocation of the unfolded Titin I27 mutant chimera into microsomes is ATP-dependent and requires functional Sec63-BiP interaction 39

Figure S1. Estimation of BiP concentration in microsomes 63

Figure S2. Components of the Sec61 translocon from microsomes of the RSY1255 yeast strain 64

Figure S3. Circular dichroism spectra of the double unfolded Titin I27 mutant chimera..... 64

Figure S4. Purification of proteins for Translocation Assays 65

Figure S5. Apo-Calmodulin pulling at different temperatures in steered molecular dynamics .. 66

Figure S6. Steered molecular dynamics (SMD) unfolding of the Ca^{2+}-bound Holo-calmodulin N-lobe EF-hand domain at 20 °C and 30 °C..... 67

Figure S7. Microsomal functionality verified by *in vitro* translocation and glycosylation..... 68

Figure S8. Translocation assay of Top7 into microsomes 68

Figure S9. Amino acid sequence and domain organization of the chimeric Titin I27 mutant construct (227 amino acids) 69

Figure S10. Amino acid sequence and domain organization of the chimeric CaM construct (287 amino acids)..... 69

Figure S11. Amino acid sequence and domain organization of the chimeric Top7 construct (287 amino acids)..... 70

List of Tables

Table 1. Mean and SD values of chimera translocation rates shown in % of translocation per minute. 36

Table 2. Mean, SD, and P-values of maximum translocation level percentages at 20 °C and 30 °C 38

Table 3. Translocation requirements and parameters for each protein construct.. 41

Table S1. p-values of t-tests comparing chimera maximum translocation values at 20°C and 30°C 70

Table S2. Reagents used in this thesis..... 71

Table of Contents

Chapter 1 Introduction **1**

Chapter 2 Experimental design of a biophysical strategy to study the mechanism of BiP in post-translational translocation. **9**

2.2.- Yeast strain and plasmids: 10

2.1.1.- Microsomes extraction 12

2.1.2.- Development of an improved microsome extraction method 13

..... 14

2.1.3.- Estimation of BiP concentration in microsomes 15

2.2.- Chimeric Protein Constructs 16

2.2.1. Plasmid Construction and Molecular Cloning 17

2.2.2.- Expression and purification of chimeric proteins 18

2.3.- Biophysical characterization of Chimeric proteins 19

2.3.1.- Circular dichroism of unfolded Titin I27 mutant 19

2.3.2.- Molecular dynamics 20

2.3.3.- Top7 pulled by Optical Tweezer 20

2.4.- Kinetics of translocation 22

2.4.1- *In vitro* translocation and protease protection assays 23

2.5.- Determination of work and output power 25

Chapter 3 Mechanochemical Mechanism Basis of BiP-Mediated Post-translational Protein Translocation **27**

3.1.- Biophysical characterization validates the suitability of the chimeric substrates for translocation studies. 28

3.2.- Chimera proteins can be translocated i*n vitro* by using a microsome-based assay and visualized by non-radioactive means 32

3.3.- Kinetics of chimera substrate translocation into microsomes determined by protease protection assays. 34

3.4.- Temperature and protein structure stability effects on translocation 36

3.5. The kinetic rates of post-translational translocation are energy-dependent 38

3.6.- The output power of BiP is closer to that of ratchet molecular motors than to power stroke 39

Chapter 4 Discussion **42**

Chapter 5 Conclusions **49**

References **51**
APPENDIX A Supplemental Material **63**
Sequence of chimeric proteins 69
Titin I27 mutant chimera 69
CaM chimera 69
Top7 chimera 70
APPENDIX B Response to Reviewer Comments **72**

Chapter 1

Introduction

The secretory pathway is crucial for eukaryotic cells because it synthesizes, processes, and exports proteins to their destinations (Palade, 1975; Sánchez et al., 2025). Dysfunction in this pathway can lead to a range of significant human diseases, from congenital disorders to cancer (Feizi et al., 2017; Sánchez et al., 2022). Protein targeting to the Endoplasmic Reticulum (ER) occurs through two mechanisms: co-translational, in which the nascent polypeptide is translocated while it is being synthesized by the ribosome, and post-translational, in which the fully synthesized polypeptide is translocated after its release from the ribosome (Zimmermann et al., 2011).

In this Thesis, we focus on post-translational translocation because it remains incompletely understood. In *Saccharomyces cerevisiae*, 40% of protein translocation occurs through post-translational mechanisms (Ast et al., 2013). This is essential because other organelles, such as chloroplasts and mitochondria, also rely on this process as their primary means of protein translocation. (Ast et al., 2013; Craig, 2018; Mori & Cline, 2001; Shan, 2023). The Sec61 channel (or translocon) is the central component of the protein translocation machinery in the ER, through which polypeptides are translocated across the ER membrane. The Sec61 complex in S. cerevisiae consists of the trimeric Sec61 complex (Sec61, Sbh1, Sss1) and the tetrameric Sec62/Sec63 complex, which includes Sec62, Sec63, Sec71, and Sec72 (**Figure 1**) (Wu et al., 2019).

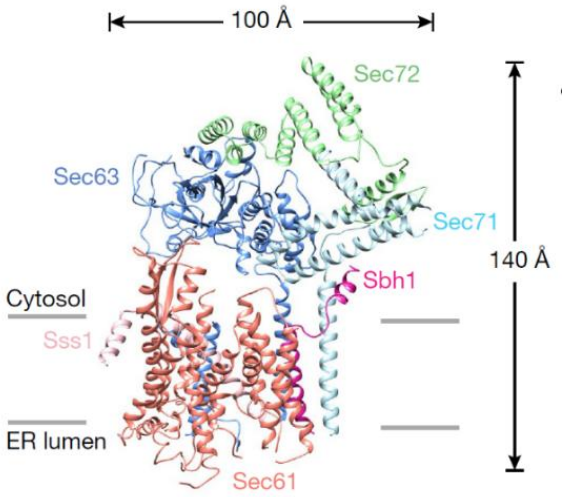


Figure 1. Structure of the Sec complex by Cryo-EM. Ribbon diagram of the Sec61 complex, obtained through cryo-electron microscopy of Saccharomyces cerevisiae. This complex primarily consists of the proteins Sec61 (53 kDa), Sec71 (40 kDa), Sec72 (22 kDa), Sec63 (75 kDa), Sss1 (9 kDa), and Sbh1 (9 kDa). The expanded data also includes Sec62 (31 kDa). Additionally, the figure shows the size of the 2D complex in angstrom (Å) units. Figure from Wu et al., (2019).

During post-translational translocation, the nascent protein is maintained in an unfolded state in the cytoplasm by chaperones of the type Hsc70 (Deshaies et al., 1988). A signal sequence (SP) present at the N-terminus of the polypeptide directs it to the endoplasmic reticulum, allowing for its recognition and subsequent translocation through the Sec61 complex into the ER lumen (Ng et al., 1996; Sánchez et al., 2026). The SP not only targets the protein to the ER but also plays a crucial role in activating the Sec61 channel. It does so by inserting into a hydrophobic pocket within the translocon's lateral gate, promoting conformational changes that allow the polypeptide to enter the channel and begin translocation (Itskanov & Park, 2023; Park & Rapoport, 2012).

BiP, an HSP70 family chaperone localized in the ER lumen, interacts with the J-domain of the Sec62/Sec63 complex, which is associated with Sec61 (M. Alfaro-Valdés et al., 2019; Pobre et al., 2019; Quiroga-Roger et al., 2022; Scidmore et al., 1993). The interaction between BiP and the J-domain of Sec63 has been shown to reduce BiP's substrate specificity, enabling it to bind more broadly along the polypeptide chain during

translocation. In contrast, BiP in solution, in the absence of Sec63, preferentially recognizes a defined consensus motif, Hy(WX)HyXHyXHy, where Hy represents a bulky aromatic or hydrophobic residue, W is tryptophan, and X is any amino acid (Blond-Elguindi, 1993).

This shift in binding behavior highlights the J-domain's modulatory role in expanding BiP's substrate recognition during post-translational translocation. BiP's activity depends on an ATPase cycle. ATP binding keeps the lid open and maintains low substrate affinity. At the same time, ATP hydrolysis to ADP closes the lid and increases affinity for the polypeptide (McCarty et al., 1995). **Figure 2** summarizes the main steps and components involved in this process.

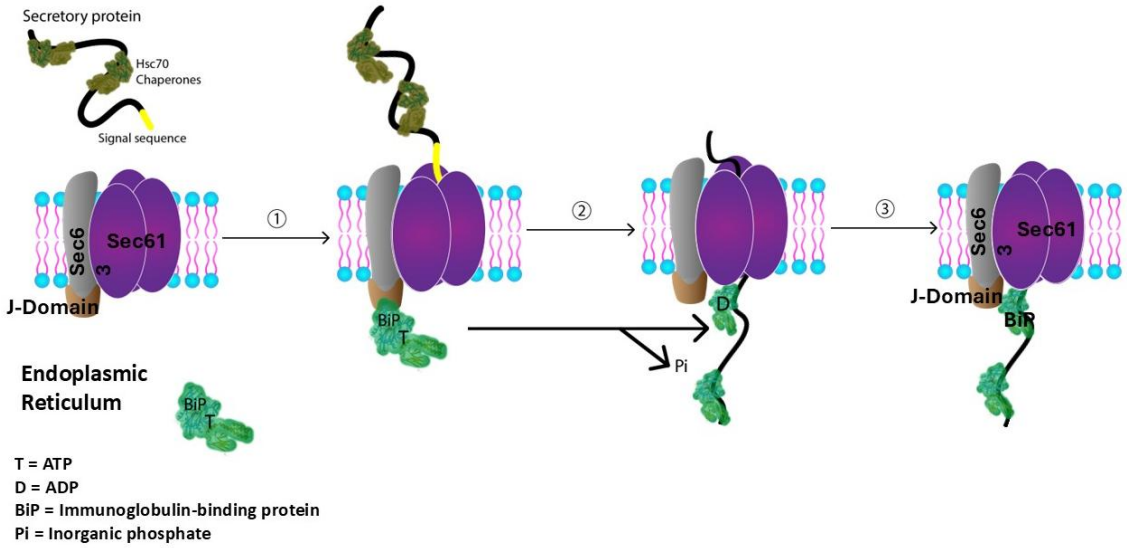


Figure 2. Scheme of the post-translational process of secretory protein in eukaryotic cells. The protein interacts with Hsc70 chaperones that keep it unfolded and ready for translocation. Sec61 recognizes the signal sequence of the protein (in yellow) and binds to the channel. Inside the ER, the J domain of the Sec62/Sec63 complex interacts with BiP. BiP binds to the incoming polypeptide chain through ATP hydrolysis, facilitating its entry into the ER. PDB of BiP 5e84.

The prepro-alpha-factor (ppαF) from *S. cerevisiae* was the first eukaryotic protein described to exhibit this post-translational mechanism (Hansen et al., 1986). Its SP contains the canonical features required for ER targeting and efficient engagement with

the Sec61 complex. A single-molecule optical tweezers study showed that the SP of ppαF interacts with the Sec61 complex for up to 17 seconds (Robeson et al., 2024; Sánchez et al., 2026). Based on the reported association rate constant, k_{on}, of BiP to its substrate protein, which ranges between 0.01 and 0.001 $\mu M^{-1} \cdot s^{1}$, and BiP intracellular concentration in the millimolar range (Sánchez et al., 2022), the ~17-second window of signal sequence interaction with the translocon is sufficient to allow BiP binding and action (Ramírez et al., 2017).

From both biological and biophysical perspectives, BiP has been proposed to function as a molecular motor during post-translational translocation into the endoplasmic reticulum (ER) (Matlack et al., 1999). However, its precise mode of action remains under active investigation. Two principal mechanistic models have been suggested. In the passive Brownian ratchet model, BiP utilizes ATP binding and/or hydrolysis to rectify thermally driven fluctuations of the polypeptide chain, resulting in a net unidirectional movement without directly exerting mechanical force (Astumian, 1997; Glick, 1995; Matlack et al., 1999).

In contrast, the power stroke model posits that BiP converts the chemical energy released from ATP hydrolysis into mechanical work, actively pulling the substrate into the ER (**Figure 3**). In this case, BiP would perform work greater than the thermal energy (approximately $3k_BT$, where k_B is Boltzmann's constant and T is the absolute temperature) (Smith et al., 2001). These models imply different levels of mechanical output and the timing of substrate engagement. Here, it is important to mention that, according to the Equipartition Theorem, the thermal energy of a system with 6 degrees of freedom (3 translational and 3 vibrational) corresponds to $3k_BT$ (Greiner et ., 1995).

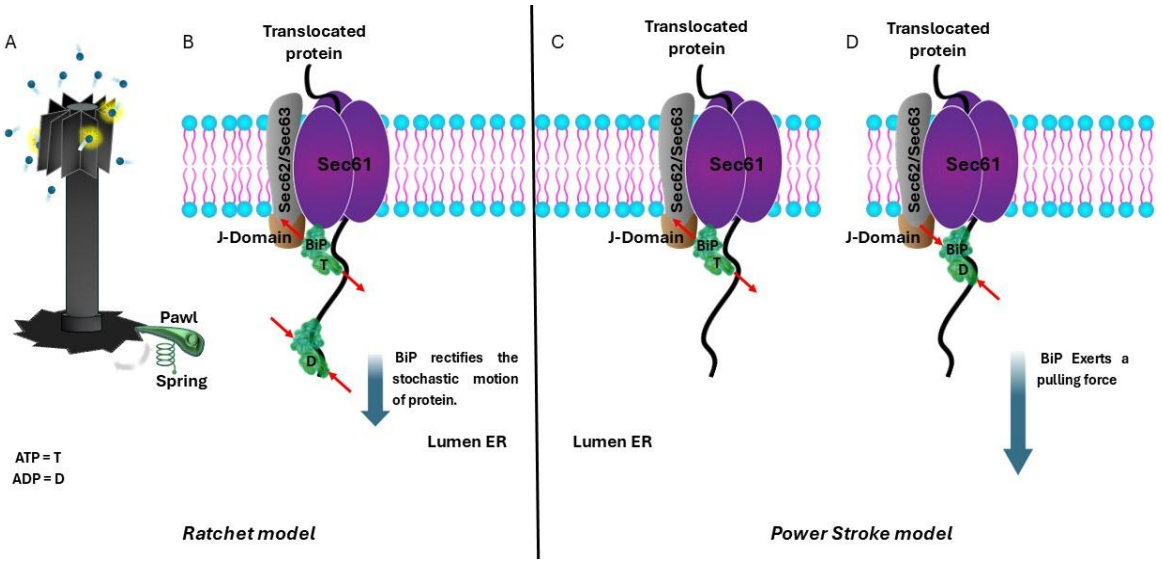


Figure 3. Mechanochemical mechanism of BiP function during post-translational translocation. These models explain how the chaperone BiP converts chemical energy derived from ATP hydrolysis into mechanical force, driving protein translocation through the Sec61 channel in the endoplasmic reticulum. **(A) Ratchet model**. The ratchet represents the translocating protein (shown in black), the pawl corresponds to BiP, and the spring symbolizes ATP (depicted in green). **(B)** The BiP ATPase cycle regulates substrate affinity by alternating between the open-domain, ATP-bound (T) conformation and the closed-domain, ADP-bound (D) conformation. **(C)** Power stroke model with BiP in the open-domain conformation, characterized by low substrate affinity, which allows freer polypeptide movement through the channel. **(D) Power stroke model** with BiP in the closed-domain conformation following ATP hydrolysis, generating a mechanical force that actively drives the polypeptide into the lumen. The length of the arrow corresponds to the translocation rate, with shorter arrows indicating slower kinetics and longer arrows faster kinetics. Adapted from Wilson et al. (2025).

Although the Brownian ratchet model has received substantial experimental support, these studies have not completely excluded the possibility that BiP can also contribute to translocation through active mechanical pulling. For example, Matlack et al. (1999) used a soluble translocation system and replaced BiP with antibodies against prepro-alpha-factor (ppαF), showing protein translocation, albeit at much slower rates, suggesting that binding prevented backward movement (Matlack et al., 1999). Similarly, by examining translocation step size and substrate unfolding states, Yamano et al. (2008) showed that the ratchet mechanism is sufficient to drive protein movement into mitochondria by mtHsp70 (Yamano et al., 2008). This suggests that BiP's ratchet activity would be sufficient to translocate proteins into the ER. Although these studies provide

sufficient experimental evidence to support the ratchet mechanism, they have not ruled out the possibility that BiP could exert some degree of active pulling in cases of tightly bound or folded mature proteins. Thus, whether BiP functions exclusively as a Brownian ratchet or can also generate active mechanical work remains unresolved.

Early computational modeling studies suggested that BiP can exert a 10–15 pN force during substrate interaction, causing pulling across membranes and enabling efficient translocation (De Los Rios et al., 2006; Rukes et al., 2024). From these findings, a model of entropic pulling has been proposed to explain the BiP mechanism. In this model, translocation is initially fuelled by thermal fluctuations and BiP ratchet action, with the resultant conformational changes of the translocating peptide and increasing spatial restrictions changing the free energy available to the system and thereby thermodynamically favoring substrate pulling. This model can explain why some studies showing ratchet-type behavior of BiP demonstrate the ability to mediate translocation but may not be sufficient to translocate peptides with the efficiency seen under physiological conditions.

However, concurrent cellular events within the endoplasmic reticulum, such as glycosylation, may modulate this process (Trombetta, 2003). Moreover, the combination of BiP activity and glycosylation may exert a synergistic effect, resulting in more efficient and faster translocation kinetics compared to either mechanism alone. In this context, understanding BiP's role as passive or active, and how it interacts with other ER-resident processes such as glycosylation, is key to interpreting how mechanical forces and conformational changes influence the efficiency of protein maturation and post-translational modification within the ER (Wilson et al., 2025).

To rigorously distinguish between passive ratcheting and active power-stroke mechanisms, force alone, however, does not fully describe BiP's mechanical contribution during protein translocation. The mechanical work (W) performed during translocation depends on both force and displacement ($W=F \times D$; (Serway et al., 2014)). In this context,

fluorescence measurements have estimated a ~1-nm displacement between BiP's NBD and SBD domains (Marcinowski et al., 2011), whereas an effective step size of ~2.4 nm has been proposed based on the minimum polypeptide length required to span the distance from the BiP binding site and the Sec61 channel (>7 amino acids assuming 0.34 nm per residue) (Yamano et al., 2008). Together with our force measurements, these displacement values allow us to estimate the mechanical work performed by BiP during translocation.

Mechanical output power (*P*), the rate at which a mechanical system generates useful mechanical energy over time (Serway et al., 2014), provides an additional metric for distinguishing active power-stroke mechanisms from passive ratcheting. Power-stroke motors actively perform mechanical work and therefore generate higher mechanical power, whereas passive motors are expected to have lower power output (Bustamante et al., 2004). Estimating mechanical power also requires the translocation rate ($P = F \times v$). Together, measurements of force, displacement, and translocation kinetics allowed us to quantify the mechanical work and power generated by BiP and assess whether its behavior is more consistent with a ratchet or power-stroke mechanism.

Dissecting this coordination requires evaluating how BiP activity is synchronized with the Sec61 translocation channel. Researchers studied post-translational translocation in microsomes from *Saccharomyces cerevisiae*, a fragmented endoplasmic reticulum, to evaluate the efficiency of protein ppαF translocation. Research by Nelson et al. (1993) employed sequencing analysis to identify that a yeast strain exhibiting defects in post-translational translocation harbors a mutation in which alanine (A) 179 is replaced by threonine (T) in the J domain of Sec63 (Nelson et al., 1993). Because this mutation alters the interaction between BiP and Sec63, it is key to analyzing coordination defects that directly affect translocation kinetics and determining whether process velocity is limited by molecular-motor activity or channel properties. Although BiP has been proposed to function as a ratchet-like molecular motor during post-translational translocation, the regulation of its activity before substrate engagement remains poorly understood. Its interaction with the J-domain of Sec63, which stimulates BiP's ATPase activity, appears

critical for synchronizing its functional cycle and may modulate its substrate affinity.

In summary, studying post-translational translocation from both biophysical and biochemical perspectives is essential to uncover the underlying mechanisms that govern it. Bulk measurements are essential for determining global kinetic and physical parameters. Here, we developed a novel bulk-phase methodology based on an *in vitro* yeast microsome protease-protection assay to measure the translocation of chimeric substrates with different unfolding forces to estimate the force generated by BiP.

The protein constructs used in this study are designed to include a signal peptide recognized by Sec61, followed by the unfolded Titin I27 mutant to allow microsomal entry, and finally the protein of interest Top7 (high unfolding force) or Calmodulin (CaM, low unfolding force), whose unfolding forces have been previously characterized using optical tweezers (Goldman et al., 2015; San Martín et al., 2017). Complementing this approach, we also aim to kinetically characterize the interaction between BiP and the J domain *in vitro* using the strain mutant. Mechanochemical studies of BiP in this context open new avenues for elucidating the molecular details of its interaction with the Sec61 translocon, which is essential for understanding its role in driving translocation and its impact on the efficiency and kinetics of substrate import into the endoplasmic reticulum.

This thesis is organized as follows: **Chapter 2** presents the research methodology, including all materials and methods. **Chapter 3** presents the main results of this thesis, focusing on the mechanochemical mechanism of BiP and elucidating the type of molecular motor it represents using results obtained with the methodology described above. Then, **Chapter 4** discusses the results, and **Chapter 5** summarizes the main conclusions.

Chapter 2

Experimental design of a biophysical strategy to study the mechanism of BiP in post-translational translocation.

In this chapter, we describe a novel methodological framework to estimate the mechanical forces generated by the molecular motor, BiP, that drives post-translational translocation. This strategy combines a chimeric protein containing a defined unfolding force previously established in the literature by optical tweezers. We generated chimeric proteins and evaluated import through an *in vitro* protease protection assay using yeast microsomes from *Saccharomyces cerevisiae*. The objective is to determine translocation kinetics and estimate the substrate translocation velocity (**Figure 4**). This chapter therefore describes the development of an improved, scalable method for obtaining microsomes for *in vitro* translocation assays. It describes the design and characterization of chimeric protein substrates with different unfolding forces and the experimental procedures used to quantify translocation efficiency over time and determine translocation rates.

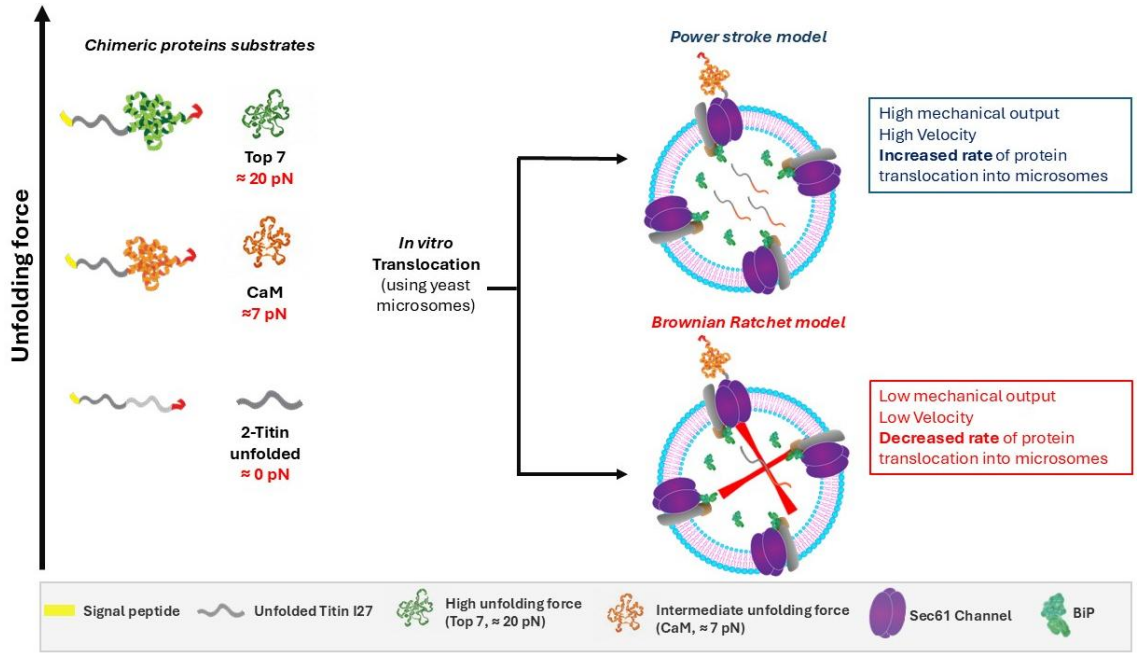


Figure 4. Experimental model to investigate the mechanochemical mechanism of BiP in posttranslational translocation by protease protection assay. Schematic representing the experimental design using a chimeric protein containing: the signal sequence (yellow) recognized by the Sec61 complex; an unfolded protein called the unfolded Titin I27 mutant (gray); and a folded protein with a known unfolding force measured using optical tweezers. A protein with low unfolding force (CaM, ≈ 7 pN) and another with high unfolding force (Top7, ≈ 30 pN) will be used. Finally, we will add a histidine tail (red) to purify the protein. We will use this chimera in an *in vitro* protection assay with yeast microsomes to determine whether BiP can exert sufficient force to unfold and translocate the chimeric substrate. Suppose translocation of the low-unfolding-force combined with exclusion of the high-unfolding-force indicates a Brownian ratchet mechanism. On the contrary, if both (the low- and high-unfolding-force) translocate, it would suggest an active power stroke-type motor mechanism.

2.2.- Yeast strain and plasmids:

The *Saccharomyces cerevisiae* strain RSY1255, which carries a chromosomal deletion of SEC61 complemented by the centromeric plasmid pDQ1 (LEU2) expressing His_6-tagged Sec61, was generously provided by the Schekman Laboratory and utilized for translocation kinetics assays (Lyman & Schekman, 1995).

To analyze the BiP–Sec63 interaction, a strain harboring a mutation at a conserved alanine within the J-domain of Sec63, which destabilizes the BiP–Sec61 complex association (Misselwitz et al., 1999), was constructed using a plasmid-shuffling strategy (**Figure 5**). To facilitate downstream purification of both wild-type (WT) and mutant variants, a FLAG tag was fused to the C-terminus of Sec63. The parental strain Emy159 (MATa, ura3-52, lys2-801am, ade2-101oc, sec63Δ::kanMX) features a genomic deletion of SEC63 complemented by a centromeric pRS316 plasmid (URA3) expressing WT ScSEC63-FLAG under its endogenous promoter.

This strain was transformed with either pRS315 (LEU2) ScSEC63-FLAG-WT or pRS315 (LEU2) ScSEC63-FLAG-A179T, where the conserved alanine is substituted with threonine to disrupt BiP interaction. We selected transformants on synthetic defined double-dropout media lacking leucine and uracil (SD–Leu–Ura) at 24 °C for 3 days to maintain both plasmids simultaneously. We pooled multiple transformant colonies, restreaked them onto SD–Leu–Ura plates, and then resuspended equal cell densities in sterile water and plated them onto SD–Leu agar plates supplemented with 1 g/L 5-fluoroorotic acid (5-FOA, Sigma) and uracil. This counterselection eliminates Ura^+ cells, forcing the loss of the original pRS316-WT plasmid and leaving the sec63Δ genomic knockout exclusively complemented by the pRS315-borne WT or sec63-A179T allele.

Because the sec63-A147T mutation is temperature-sensitive, displaying a WT phenotype at the permissive temperature (25 °C) and a mutant phenotype at the restrictive temperature (37 °C), and the complete absence of functional Sec63 is lethal, all plasmid replacement steps were strictly conducted at 25 °C. Complete loss of the pRS316 plasmid was verified by lack of growth on SD–Leu–Ura double-dropout control plates. We extracted plasmids from the resulting strains and confirmed the mutation by DNA sequencing. The Tom Rapoport Laboratory (Harvard University) kindly provided strains and plasmids for further functional characterization (Wu et al., 2019).

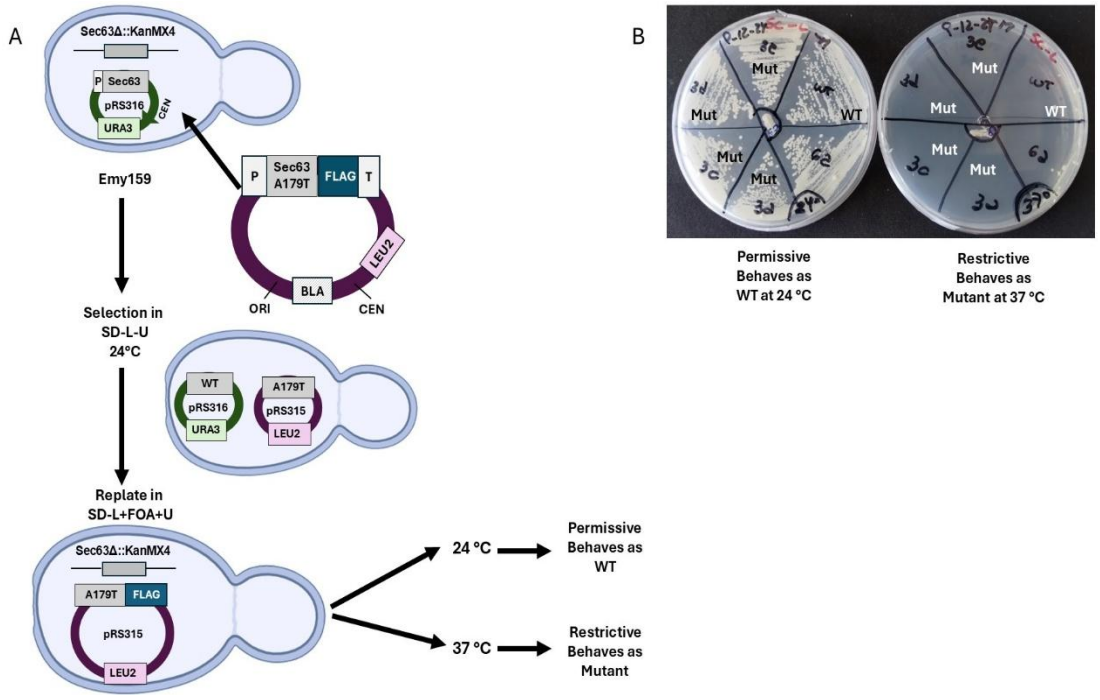


Figure 5. Generation of the yeast Sec63 (A179T) mutant. (A) Schematic workflow of the plasmid shuffling procedure in the *S. cerevisiae* Emy159 strain (*sec63Δ::KanMX4* complemented by *pRS316-Sec63-WT* [*URA3*]). Cells were transformed with *pRS315-Sec63(A179T)-FLAG* [*LEU2*] (as well as a *pRS315-Sec63(WT)-FLAG* control plasmid). We selected transformants on SD-Leu+Ura plates at 24°C and counter-selected them on 5-fluoroorotic acid (5-FOA) plates supplemented with uracil to eliminate the *URA3* helper plasmid. **(*B*)** Growth assay of the resulting yeast strains on selective SD-Leu media at permissive (24 °C, left) and restrictive (37 °C, right) temperatures. Both the wild-type (WT) control and the isolated *sec63(A179T)* mutant candidates (Mut) grow at 24 °C. In contrast, at 37 °C, the mutant strains show no growth, confirming that the *sec63(A179T)* allele confers a temperature-sensitive lethal phenotype.

2.1.1.- Microsomes extraction

We initially extracted microsomes from *Saccharomyces cerevisiae* according to the Lyman and Schekman protocol (the Schekman method, MS). In parallel, we designed an improved method combining two techniques for microsome extraction to reduce preparation time and costs, improve yield, and maintain purity. This method improves the Parodi method (MP), which first obtains a microsomal fraction (Fernández et al., 1994), followed by the final purification step of the MS, which consists of a sucrose gradient. After differential centrifugation, the microsomes are obtained by density (**Figure 5**). This

new method is cheaper, faster, and requires less preparation time than MS, which requires preparing several buffer solutions and a high-activity lyticase enzyme. Furthermore, adding the final MS step yields purer microsomes. We obtained microsomes from different yeast strains, as described below.

2.1.2.- Development of an improved microsome extraction method

We extracted microsomes from Saccharomyces cerevisiae according to the protocol of Lyman and Schekman (1995) and by combining two methods with modifications: Parodi and Schekman (Fernández et al., 1994; Lyman & Schekman, 1995), as shown in **Figure 6**. The method was scaled up from 1 L to 4 L, and cells were grown to an OD_{600} of 5-7. They were then harvested at 4550 × g, 4 °C for 10 min. The pellet was then washed with 150 mL of 5 mM sodium azide (NaN_3).

Then the pellet was resuspended in Solution A (20 mM imidazole buffer pH 7.5, 0.25 M sucrose, and 5 mM EDTA) at a ratio of 2 ml/g of pellet, supplemented with protease inhibitors: 1 mM PMSF (Sigma), 1 µM pepstatin (Sigma), 1 µM leupeptin (Sigma), 1 µM TLCK (Sigma), and 1 µM E-64 (Sigma). We disrupted the sample by adding one volume of glass beads and subjecting them to 10 disruption cycles: 1 minute of vortexing followed by 1 minute of incubation on ice. Next, centrifuge the sample for 10 minutes at 3,000 x g at 4 °C, then collect the supernatant. Two milliliters of Solution A were added to the pellet, and another 10 disruption cycles were performed as previously described.

The resulting supernatant was pooled with the previous supernatant, then centrifuged at 4,000 x g for 10 minutes at 4 °C. The new supernatant was then ultracentrifuged at 100,000 x g for 1 hour at 4 °C. The resulting pellet (ER-enriched microsomal fraction) was resuspended in B88 buffer (20mM HEPES pH 6.8, 250mM sorbitol, 150mM KOAc, 5mM Mg(OAc)2) supplemented with protease inhibitors at a ratio of 250 µL of buffer per 250 mL of culture.

Then, we added the final step of the method (Lyman & Schekman, 1995) to obtain purified microsomes. We purified the microsomal membranes by sucrose gradient centrifugation using 1.2 M and 1.5 M sucrose solutions in 20 mM HEPES (pH 7.5), 50 mM potassium acetate (KOAc), and 2 mM EDTA.

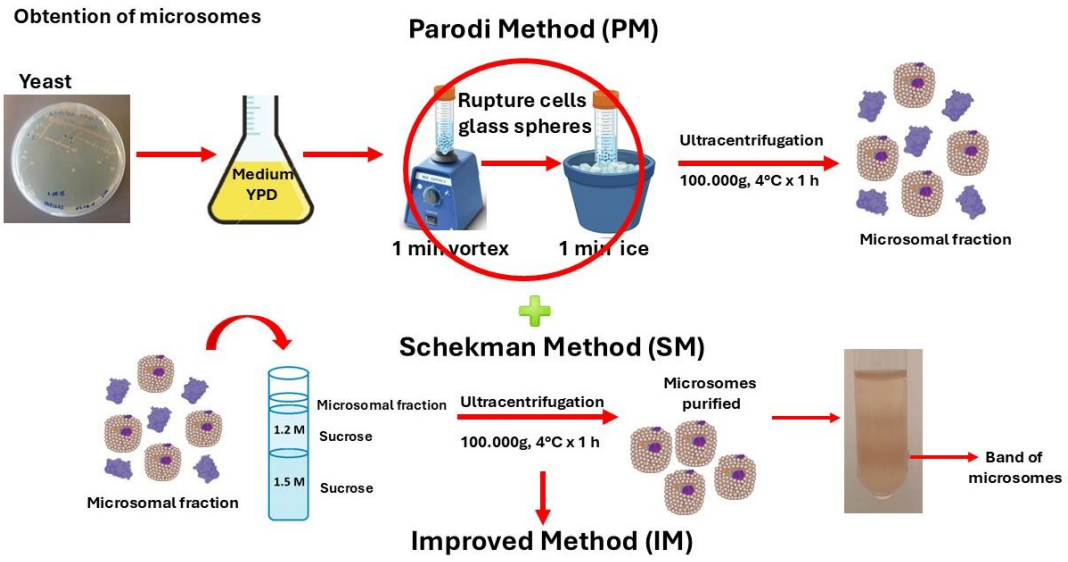


Figure 6. Schematic of the development of an improved method for isolating yeast microsomes by combining the Parodi and Schekman methods. The schematic shows IM extraction from yeast strain RSY1255, which contains a histidine tag for purification, or a strain expressing the mutant Sec63 protein tagged at the C-terminus with a FLAG tag used in this thesis. Harvest the culture for extraction from 250 mL of YPD medium. Next, mechanically disrupt cells using glass beads by vortexing for 1 minute, then 1 minute on ice. Ultracentrifugation at 100,000 × g is then performed to obtain a microsomal fraction; this first part corresponds to the Parodi method. The final step of the Schekman method (Lyman & Schekman, 1995) is then added to the Parodi method (Fernández et al., 1994), which consists of adding the microsomal fraction to a sucrose gradient. Purified microsomes are obtained after ultracentrifugation at 100,000 × g. The band collected corresponds to the higher density at the bottom of the sucrose gradient.

Then, we performed one ultracentrifugation in an SW55 rotor at 100.000 × g for 1 h in a Beckman centrifuge and recovered microsomal membranes from the interface of the gradient (higher-density band; **Figure 6**, last step). Dilute the microsomal membrane 5X with buffer B88 and centrifuge at 26700 × g for 10 min at 4 °C using a Ti90 rotor (Beckman centrifuge).

Discard the supernatant and resuspend the pellet in approximately 1 mL of Buffer B88. When needed, add a small additional volume of B88 to obtain a good resuspension of microsomal membranes while maintaining a high microsomal concentration. The concentration of microsomal membranes was determined by absorbance at 280 nm (A_{280}) by diluting 5 µL of microsomal membranes in 995 µL of 2% SDS (200-fold dilution). We then calculated the concentration as $A_{280} \times 200$. To confirm the components of the Sec61 translocon, we performed Western blotting with specific antibodies against Sec61, Sec63, Sec72, and BiP.

We confirmed the presence of the channel components (**Figure S2**). Primary antibodies against each protein of interest were provided by the laboratory of Dr. Randy Schekman at the University of California, Berkeley. The dilutions used for each antibody were as follows: 1:5000 for Anti-Sec61, 1:10000 for Anti-Sec63, 1:500 for Anti-Sec72, 1:10000 for Anti-BiP, and 1:1000 for anti-rabbit IgG secondary antibody (Invitrogen, catalog number G21234). For immunodetection, we used SuperSignal West Femto reagent (Pierce Biotechnology, Inc.). We obtained images using the Dyversity 4 image capture and analysis system (Syngene).

2.1.3.- Estimation of BiP concentration in microsomes

A semi-quantitative Western Blot analysis using anti-BiP antibodies was used to determine BiP concentration in microsomes. Briefly, increasing amounts of purified BiP protein (in ng) as well as different volumes of diluted microsomes were boiled for 5 min in Laemmli buffer (2% SDS, 10% Glycerol, 62.5 mM Tris-HCl, pH 6.8, 5% β-mercaptoethanol and 0.01% bromophenol blue), separated by 10% SDS-PAGE gels, transferred onto nitrocellulose membrane, and blocked in 5% w/v non-fat, dry milk in PBS containing 0.1% Tween-20.

Immunoblots were analyzed by incubation of membranes with anti-BiP antibodies (as above) for 1 h at room temperature. Membranes were then washed and incubated with

horseradish peroxidase-conjugated goat anti-rabbit IgG (1:3000; G21234, Invitrogen) for 1 h at room temperature. Peroxidase activity was detected using a chemiluminescence kit (Pierce, Thermo Scientific). We generated a standard curve based on signal intensity by increasing the amount of pure BiP loaded in the gel (**Figures S1A** and **S1B**). We then used the linear regression equation from the standard curve and the molecular weight of BiP (72 kDa) to quantify BiP concentration in the different volumes of microsomes analyzed (Figure S3C). Using the Packed Cell Volume tubes (Techno Plastic Products AG), we estimated that our samples contain ~50% microsomes. Thus, we corrected the BiP concentration in the microsomes by a factor of 2.

2.2.- Chimeric Protein Constructs

We engineered chimeric proteins to evaluate substrate translocation efficiency under distinct unfolding forces. All constructs contained an N-terminal signal sequence for Sec61 translocon recognition (Waters et al., 1988), followed by an unfolded Titin I27 mutant carrying two-point mutations (C47E and C63E) to prevent folding and allow initial channel entry (Goldman et al., 2015; San Martín et al., 2017).

A protein domain of interest was placed downstream of the unfolded Titin I27 mutant, followed by a C-terminal 6xHis tag for purification (**Figure 7**). To test the impact of the unfolding force, thee target domains with a similar primary structure length (~249 amino acids) were selected: (i) an additional unfolded Titin I27 mutant (without unfolded force ~ 0 pN) as a fully unfolded positive control; (ii) Calmodulin (CaM, ~7 pN) (Chattopadhyaya et al., 1992) as a test substrate with low mechanical stability (18); and (iii) Top7 (~20 pN, validated in this study) (Kuhlman et al., 2003) as a high-force negative control.

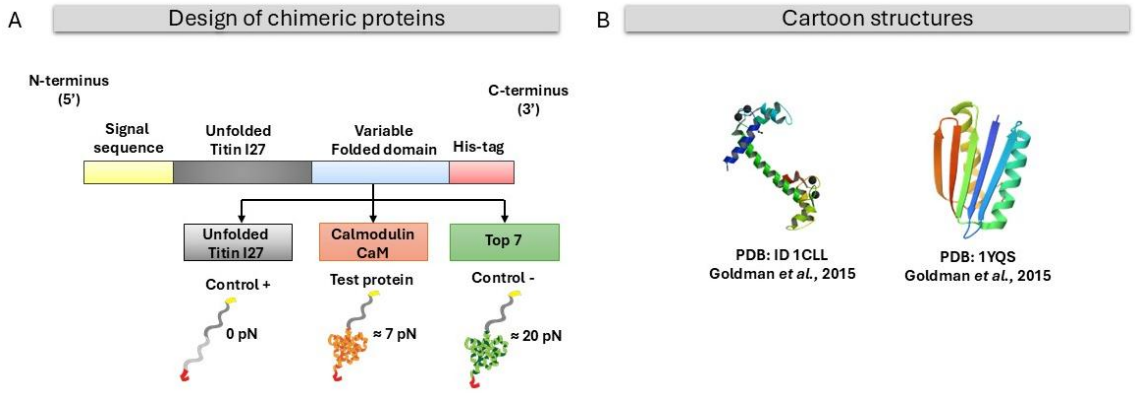


Figure 7. Schematic representation of the design of chimeric protein constructs. **(A)** Design of chimeric proteins containing two peptide domains, with an N-terminal signal sequence for post-translational translocation, followed by the unfolded Titin I27 mutant (unfolded domain of the chimeric protein competent for post-translational translocation), one variable domain for cloning unfolded protein or folded protein, followed by a C-terminal His-tag for purification. The variable domain will be substituted for either: unfolded Titin I27 mutant (zero unfolding force, positive control), CaM (7 pN unfolding force, test protein), or Top 7 (20 pN unfolding force, negative control). **(B)** Cartoon structures of calmodulin (left, Chattopadhyaya et al., 1992) and Top 7 (right, Kuhlman et al., 2003).

2.2.1. Plasmid Construction and Molecular Cloning

Plasmids containing the coding sequences for the proteins of interest were kindly provided by Prof. Carlos Bustamante (UC Berkeley; Top7 and CaM) and Prof. Mauricio Baez (University of Chile; unfolded Titin I27 mutant). Integrated DNA Technologies (IDT, USA) synthesized the full-length chimeric nucleotide sequence with unique restriction sites flanking each functional module to facilitate cloning and domain swapping. Specifically, the construct was assembled with the Sec61 signal peptide sequence between *Nco*I and *Nde*I restriction sites, the non-folding unfolded Titin I27 mutant between *Nde*I and *Bam*HI, a linker sequence between *BamH*I and *EcoR*I, the target protein sequence (folded domain) between *Eco*RI and *Xba*I, and a C-terminal 6xHis tag between *Xba*I and *Hind*III. The resulting synthetic construct was subcloned into the pET-21d(+) expression vector (Novagen) for protein expression.

2.2.2.- Expression and purification of chimeric proteins

The pET-21d(+) plasmid containing the chimeric sequence was transformed into SecY(ts) Escherichia coli cells and expressed, provided by the University of California, Los Angeles. This strain carries a temperature-sensitive mutation in the SecY channel that impairs protein secretion at non-permissive temperatures (42 °C) (Lecker et al., 1989). This restriction prevents signal-sequence cleavage during SecY-mediated secretion, preserving the intact signal peptide required for subsequent recognition of chimeric proteins by the Sec61 complex (Lecker et al., 1989).

We inoculated bacterial cultures from a saturated overnight pre-inoculum (50 mL) into 1 L of LB medium at an initial OD600 of 0.1 and grew them at 30 °C. Protein expression was induced at an OD_{600} of 0.7 with 0.5 mM IPTG for 4 hours at 42 °C. We harvested cells by centrifugation at 4080 × g for 20 min and resuspended them in lysis Buffer A (50 mM HEPES pH 7.4, 150 mM KCl, 10 mM Imidazole). We purified the chimera proteins by nickel affinity column chromatography using a 1 mL HisTrap HP column (GE Healthcare), as previously described (Ramírez et al., 2017). Protein elution was performed using a linear imidazole gradient (10 mM-100 mM), with 1 mL fractions collected.

To maintain an unfolded state during purification, we included 6 M urea in Buffer A. The ppαF control protein was performed in the presence of 8 M Urea according to Bush et al., (1991), and the protein was purified in the presence of 6 M urea (Bush et al., 1991). To maintain the unfolded state of the Titin I27 mutant chimera during purification, 6 M urea was included in buffer A. Sample purity and identity were confirmed by SDS-PAGE, and mass spectrometry was performed using trypsin or chymotrypsin digestion at the Taplin Biological Mass Spectrometry Facility (Harvard Medical School, Boston, MA).

2.3.- Biophysical characterization of Chimeric proteins

2.3.1.- Circular dichroism of unfolded Titin I27 mutant

The UV circular dichroism (CD) experiments (Greenfield, 2006) to characterize the secondary structure of the chimeric unfolded Titin I27 mutant were conducted on a Jasco 1500 spectrophotometer with an optical path length of 1mm and a protein concentration of 0.5 mg/mL. The titin chimera underwent buffer exchange via 3 rounds of concentration of the original 1 mg/mL stock using microcentrifuge concentrators with a 10 kDa molecular weight cut-off (Milipore, Darmstadt, Germany) and resuspension in 50 mM HEPES, 150 mM KCl, and 1 M urea to remove imidazole content, as this causes interference in the CD spectroscopy reading. The elute of the last of the 3 rounds of passing the sample through concentrators was also measured as a buffer-only control condition.

We obtained each spectrum by accumulating 5 scans (bandwidth 1 nm, scan rate 50 nm-1, wavelength step size 0.1 nm). The wavelength range was 210-260 nm, as the high absorbance of imidazole in the buffer did not allow recording spectra below 210 nm (**Figure S3**). The parameter reported here is the mean residue ellipticity (MRE), calculated as (Greenfield, 2006):

$$[\theta] = \frac{CD_{mdeg} \times MRW_{kDa}}{l_{mm} \times c_{mg/mL}},$$

whereby CD is the raw ellipticity value in millidegrees, MRW is the mean residue weight, l is the light path length, and c is the protein concentration.

2.3.2.- Molecular dynamics

Steered molecular dynamics (SMD) simulations were performed on the isolated N-lobe EF-hand domain of apo (PDB 1CFD) and holo-calmodulin, (PDB 1CLL). We simulated the input structures for 1 μs of all-atom equilibration at 20 °C and 30 °C using the Amber99sb-ildn force field, TIP3P water, and 0.15 M NaCl.

Starting conformations were the representative structure of the largest cluster identified by hierarchical clustering (Ward linkage, backbone RMSD, elbow-selected cluster count, TTCLUST (Tubiana et al., 2018) of their corresponding 1 μs trajectory run in Gromacs 2026 (Abraham et al., 2015). We solvated the equilibrated structure in a 5.5 × 5.5 × 18.0 nm box for CaM, then energy-minimized and thermalized under the same conditions as before, before production in OpenMM (Eastman et al., 2024).

SMD pulling held the N-terminal Cα fixed via a harmonic restraint (k = 100 kJ mol^{-1} nm^{-2}) while the C-terminal Cα was pulled along the z-axis with a moving harmonic restraint (k = 120.44 kJ mol^{-1} nm^{-2}) in OpenMM at a constant velocity of 40 nm/μs (0.04 nm/ns), requiring 330 ns for global unfolding. We ran six independent replicas for each system and temperature condition.

2.3.3.- Top7 pulled by Optical Tweezer

DNA handles preparation

We prepared DNA handles as described by Cecconi et al., with a modification in the digoxigenin handle (Cecconi et al., 2008). The DNA handles were synthesized by means of PCR in a total reaction volume of 9.6 mL using pGEMEX (Promega) The primers used were: 5' thiol-GCT-ACC-GTA-ATT-GAG-ACC-AC, 5' biotin-CAA-AAA-ACCCCT-CAA-GAC-CC and double digoxigenin /5DigN/CA AAA AAC CCC TCA AGA/iDigN/CCC (IDT), in order to prepare 2 types of DNA handles: SH-DNA-biotin and SH-DNA-digoxigenin. The SH group was incorporated to interact covalently with the

chimera protein, while the biotin and digoxigenin were used to interact with beads coated with streptavidin or anti-digoxigenin, respectively.

We purified the DNA handles using the HiSpeed® Plasmid Midi Kit from Qiagen, adding 3 mM DTT at each step. After purification, we incubated the DNA handles for 2 hours with 10 mM DTT. We then removed DTT from the sample by passing it through Micro Bio-Spin 6 columns (Bio-Rad).

Cysteine activation and DNA handles attachment

To attach the 5'-SH-DNA handles to the Top7 chimera proteins, we first activated the cysteines on the Top7 protein, as described before (Cecconi et al., 2008; Wilson, 2011). We then incubated the chimeric Top7 (100 μM) containing two cysteines (R2C/R218C) with 10 mM DTT for 2 hours at room temperature (21-23 °C). Next, the protein was passed through two Micro Bio-Spin 6 columns (Bio-Rad), pre-equilibrated with 100 μM 2,2′-dithiodipyridine (DTDP). We then added DTDP to the sample solution to reach a final concentration 25-fold higher than that of the protein and incubated the solution at 25 °C for 2 hours.

We incubated the DNA handles for 2 hours in 10 mM DTT, then removed the DTT using Micro Bio-Spin 6 columns. After the reaction, we used the same process to remove excess DTDP and DTT from the protein and DNA, respectively (Micro Bio-Spin 6 columns, Bio-Rad). Then we combined DNA handles and protein at a DNA-to-protein molar ratio of 4:1 for 4 hours at room temperature, followed by overnight incubation at 4-8°C. We purified the DNA-protein-DNA construct by nickel affinity chromatography using columns equilibrated with a buffer of 50 mM Tris-HCl (pH 7.4), 100 mM NaCl, and 0.01% Tween. Finally, the construct stock was flash-frozen in 50% glycerol and stored at -80 °C.

Protein unfolding experiments

We first mixed chimeric protein-DNA constructs with polystyrene beads coated with anti-digoxigenin antibodies (dig-beads) for 15 min at room temperature (21-23 °C (RT). We experimentally determined the optimal dilution of the protein-DNA constructs for use in optical tweezers experiments. Dig-beads were generated by coupling anti-digoxigenin antibodies (Roche) to 3.2 μm protein G-coated beads (Spherotech) (Peña-Oyarzun et al., 2021). After reacting with the protein-DNA construct, a dig-bead was placed in the optical trap and brought into close proximity to a 2.10 μm streptavidin-coated bead (Spherotech), which was held in place at the end of a pipette until a tether formed between the two beads (Ramírez et al., 2017). We performed pulling experiments at a constant velocity (100 nm/s) using a simple trap optical tweezers instrument with temperature control at 20 °C and 30 °C (de Lorenzo et al., 2015; Rivera, Mjaavatten, et al., 2023).

Data processing and analysis

We processed the data in MATLAB using the "Tweezer Analysis" program provided by Jesse Dill (Dill, 2012). For the constant-velocity pulling analysis, we determined the force and distance at which protein unfolding/refolding occurs. To determine the latter, we approximated the curve with a line before and after unfolding/refolding and measured the distance between these lines.

2.4.- Kinetics of translocation

To characterize the kinetics of post-translational translocation, we obtained microsomes using the MS or IM method and evaluated them *in vitro* with chimeric proteins that exhibit different unfolding forces. We first validated microsome function

using purified recombinant ppαF (a classical substrate for *in vitro* post-translational translocation assays). We then performed translocation assays with different chimeric substrates to determine translocation efficiency over time and calculate the corresponding translocation velocities, as described below.

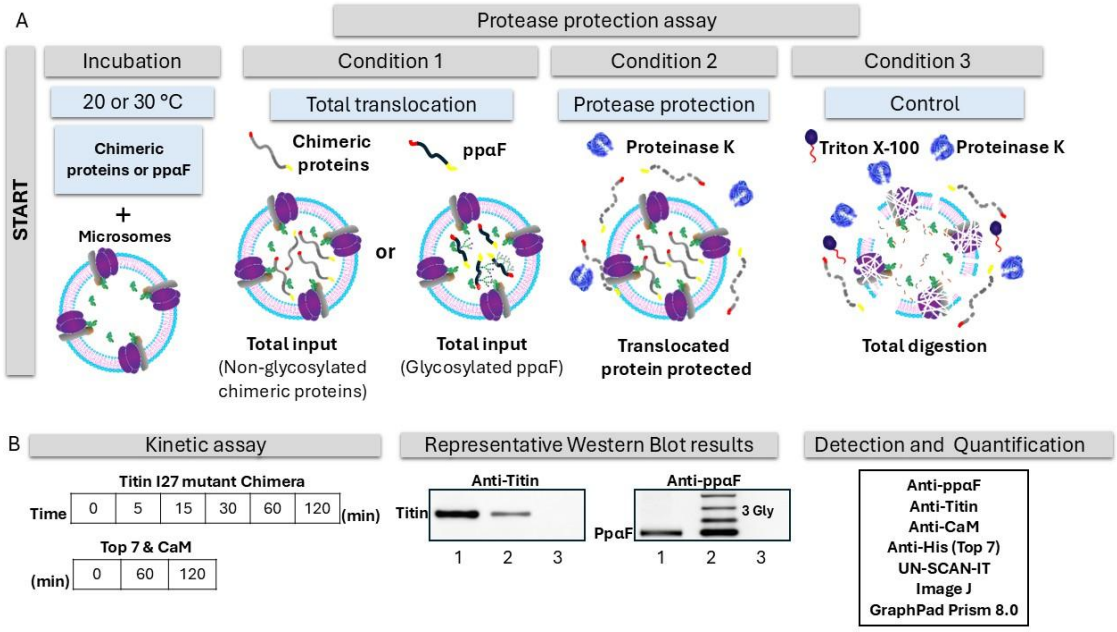


Figure 8. Schematic representation of the Translocation and kinetics analysis by Western Blot. **(A)** The translocation assay was carried out at two different temperatures and times, and then the reaction was stopped on ice. **Condition 1 (total translocation):** incubation of microsomes and protein controls or chimeric proteins. The ppαF protein validates microsome function because it is glycosylated (3Gly) when it is translocated. **Condition 2 (protease protection assay):** after incubation, proteins translocated into the microsome are protected from digestion by PK; **condition 3 (control):** Triton X-100 disrupts the microsomal membrane, allowing PK to digest all protein. We stopped protease activity with a protease inhibitor, as described by Lyman et al. (1995) or Bush et al. (1991). **(B)** The Kinetic assay was performed at different times, and detection was mediated by Western blot with an antibody specific to the protein against His-tag. We quantified results using UN-SCAN-IT or ImageJ. We analyzed the kinetics using GraphPad Prism 8.0.

2.4.1- *In vitro* translocation and protease protection assays

To test the functionality of the extracted microsomes, we carried out translocation assays as described in Lyman & Schekman (Lyman & Schekman, 1995) and Bush et al.

(Bush et al., 1991) (**Figure 8A**), with modifications to validate translocation using non-radioactive immunodetection. Microsomes were incubated for 1 hr at 20 °C or 30 °C with 3 μM chimeric proteins or with ppαF (substrates of the Sec61 complex), followed by addition of Proteinase K (PK, 0.2 mg/mL) for 30 min on ice, in the presence and absence of Triton X-100 (0.3%).

The protection condition means protease digestion of all substrates remaining outside microsomes (i.e., non-translocated substrates), so only those that have entered and are 'protected' by microsomes. We added TX-100 for 5 min as a final rest period at the end of the assay to disrupt the microsome membrane, allowing PK to degrade both the translocated and non-translocated proteins as outlined in **Figure 8A**. We stopped protease activity with a protease inhibitor (Trypsin inhibitor or PMSF). In experiments with chimeric proteins containing two domains of mutated I27 Titin or ppαF (controls), we carried out the final translocation reaction in 1 M urea to keep the protein unfolded.

Incubation times were 0, 5, 15, 30, 60, and 120 min; we stopped reactions on ice and performed protection and control tests to assess translocation kinetics. For the chimeric proteins Top7 and CaM, we conducted kinetic studies at 0, 60, and 120 min. We characterized the translocation products by SDS-PAGE and Western blotting, as outlined above (**Figure 8B**). The specific primary antibodies used were anti-histidine (1: 1,000; Abcam, catalog number AB9108), anti-CaM (1:3,000; Abcam, catalog number ab45689), and anti-ppαF (1: 10,000; provided by the laboratory of Dr. Randy Schekman of the University of California at Berkeley), and were used to bind the membrane overnight. We quantified band intensities using the UN-SCAN-IT gel 7.1 and ImageJ software (Rasband, 1997). To account for non-specific background, we subtracted the signal intensity at time zero (t = 0) and normalized the resulting values. The percentage of protein translocation is calculated as the amount of protected protein (protection condition) divided by the total quantity of protein (translocation condition), i.e., the intensity of bands obtained under protection conditions as a proportion of the intensity of bands obtained under initial translocation conditions. We performed statistical analysis using GraphPad Prism 8.0.

2.5.- Determination of work and output power

We used the mechanical work (W) performed by the molecular motor to determine whether it functions via a ratchet or power-stroke mechanism (Bustamante et al., 2004). We calculated the work as W = F x D, where F is the force (of protein unfolding), and *D* is the distance traveled (or step size of the BiP motor), assuming *F* is constant and uniform (Bustamante et al., 2004). This approximation neglects variations in the force exerted by the molecular motor but provides valuable insight into the energy the motor applies to drive movement. The surrounding thermal bath is said to have 3 k_BT of energy available, accounting for the 3 dimensions of motion, the Boltzmann constant (k_B), and the system temperature (T) (Van Holde et al., 2006). If a molecular motor can perform work greater than this, the active use of energy from ATP hydrolysis must be at play, i.e., operating according to a power-stroke model. Subsequently, any process requiring 3 k_BT or less of work may be driven by thermal fluctuations and corrected by a ratchet-type molecular motor.

In summary, the experimental strategy described in this chapter was designed to establish a robust basis for investigating the mechanism of BiP-mediated post-translational translocation through the Sec61 complex. This approach combined an optimized method developed in this work for isolating highly functional yeast microsomes with *in vitro* translocation assays. The chimeric substrate control (two unfolded Titin I27 mutants) exhibited force 0, the principal control that validates our methodology. This allows us to measure kinetics at defined unfolding forces and quantitatively analyze translocation kinetics.

Together, these methodologies provide the foundation for systematically evaluating translocation efficiency and velocity under different conditions. They also provide the experimental framework needed to investigate whether BiP can exert a larger

force than the thermal bath and to determine which of the two proposed BiP models is correct. Together, these methodologies establish the basis for mechanistic analysis, and the results obtained using this experimental platform are presented and discussed in the following chapter.

Chapter 3

Mechanochemical Mechanism Basis of BiP-Mediated Post-translational Protein Translocation

This chapter presents experimental results investigating the mechanochemical mechanism by which BiP mediates post-translational protein translocation through the Sec61 channel. To answer this question, we developed a novel experimental methodology based on a chimeric substrate design competent for post-translational translocation, with the unfolding force established in the literature using optical tweezers. Analysis of *in vitro* translocation kinetics allowed us to investigate how substrate unfolding force affects translocation efficiency and velocity.

To this end, we optimized microsome isolation from *Saccharomyces cerevisiae* and established quantitative translocation kinetics assays. We then performed biophysical characterization using circular dichroism (unfolded Titin I27 mutant chimera), optical tweezers (Top7 chimera), and steered molecular dynamics simulations (apo-CaM). Together, these approaches provide an experimental basis to evaluate the BiP mechanism and discriminate between two proposed "Brownian ratchet" or "power stroke" models for understanding BiP's contribution to post-translational translocation.

3.1.- Biophysical characterization validates the suitability of the chimeric substrates for translocation studies.

To perform the *in vitro* translocation assay, we designed and purified chimeric substrate proteins for the Sec61 complex with varying unfolding forces. As shown in **Figure 7A**, they consist of an N-terminus with a signal sequence, the unfolded mutant I27 domain of the unfolded Titin I27 mutant, the folded protein of interest (e.g., Top7 or CaM; **Figure 7B**), and a C-terminus with a His-tag for purification. We assessed purity and molecular weight by SDS-PAGE and visualized by Western blotting and Coomassie staining, obtaining bands of the expected sizes for all chimeric proteins and ppαF (**Figure S4**). Mass spectrometry corroborated the proteins' identities, indicating successful expression and purification and confirming the samples' suitability for subsequent translocation assays. Mass spectrometry analysis also confirmed the presence of the signal sequence at the N-terminus.

To confirm that mutations in the unfolded Titin I27 mutant prevent folding, we performed far-UV circular dichroism (CD) spectroscopy to assess secondary-structure content. The unfolded Titin I27 mutant chimera showed a characteristic spectrum of denatured protein conformations or disordered secondary structure, without any α-helix or β-sheets minima characteristic of folded proteins (**Figure S3**). Together, these results confirm that the unfolded Titin I27 mutant construct is fully unfolded and competent for our *in vitro* translocation studies.

To determine the mechanical stability of the folded domain of the Top7 chimera, we performed a single-molecule optical tweezers assay by pulling the protein from both its N- and C-termini (**Figure 9**). The forces required to unfold Top7 have been previously reported, with two characteristic unfolding events (also called “rips”) (Li et al., 2021).

Here, we pulled the Top7 chimera from its N- and C-termini (**Figure 9A**). As shown in **Figure 9B**, the mechanical unfolding of the chimeric Top7 protein shows two

unfolding events (also called “rips”), as previously reported for the unfolding of Top7 (Li et al., 2021). As shown in **Figure 9B**, the mechanical unfolding of the chimeric Top7 protein by optical tweezers shows those two reported rips, confirming that in our chimeric protein constructs only the Top7 domain can be mechanically unfolded in the assay. This also confirms that the Titin domain is unfolded and that no other unfolding event can be observed in that region of the chimera. We characterized the mean force of the Top7 chimera at 2 temperatures (20 °C and 30 °C): the protein was pulled 226 times at 20 °C, showing a mean force of 20.0 ± 0.3 pN, and 129 times at 30 °C, with a mean force of 19.7 ± 0.2 pN.

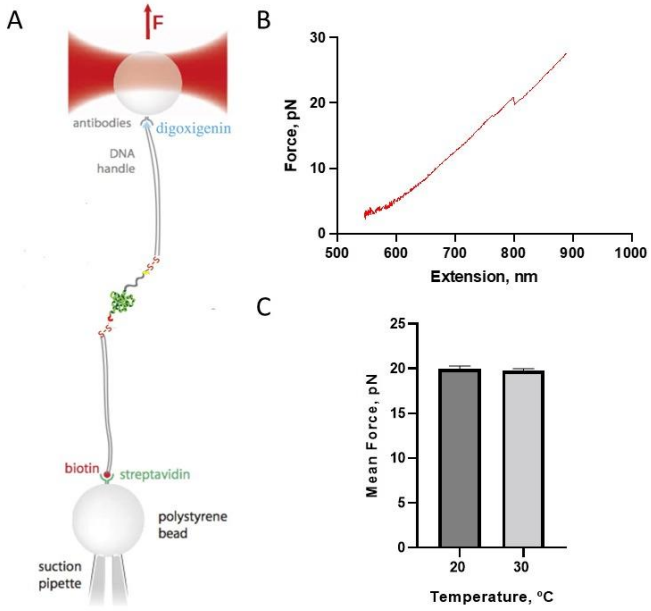


Figure 9. Experimental optical tweezers set up for the unfolding of the chimeric Top 7 protein. **(A)** The substrate protein chimera Top 7 is tethered between two dsDNA handles through disulfide bonds at its N- and C- terminus. These DNA handles are modified at the 5′ ends with either 2 digoxigenin molecules or 1 biotin to bind the polystyrene beads 3.1 and 2.1 mm) coated with anti-digoxigenin or streptavidin, respectively. The anti-digoxigenin bead is held in an optical trap, and the streptavidin bead is attached to a micropipette by suction. **(B)** Force-extension curves showing a representative pulling of chimera Top 7 at a constant speed of 100 nm/s. Unfolding events denoted by arrows at ~ 760 nm (intermediate) and 800 nm (full unfolding). **(C)** Comparison of the mean unfolding force of chimera Top 7 unfolding at 20°C and 30°C. The protein is pulled 226 times at 20°C, showing a mean force of (20.0 ± 0.3) pN, and 129 times at 30°C, with a mean force of (19.7 ± 0.2) pN.

To investigate how temperature and a state free of calcium (Ca^{2+}) influence the mechanism of CaM unfolding during translocation, we performed steered molecular dynamics (SMD) simulations on the apo- and holo- states of calmodulin. The simulations show that unfolding of the N-terminal region of apo-CaM at 20 °C is slower than at 30 °C, with different intermediate states, as shown in **Figure 10A**, **B**, and **C**. The results showed that at 30 °C, helix 1 (residues 7 to 21), the first motif to unfold, exposes hydrophobic residues to solvent earlier than at 20 °C. Although pulling at a much higher rate, these results show that destabilizing the CaM structure facilitates translocation via local unfolding at the N-terminus, reducing structural resistance at the channel entrance and allowing BiP to engage and translocate the destabilized substrate without unfolding the global protein structure.

When pulling the N-terminal lobe of CaM alongside the bound Ca^{2+} ions (holo-CaM), it can be observed that the force curve, hydrophobic sidechain exposure, and number of native contacts become indistinguishable across temperatures (**Figure S5**). Comparison of the unfolding trajectories of apo- and holo-CaM (**Figure 10D**) shows that after global unfolding, secondary structure elements remain in holo-CaM, specifically around the Ca^{2+} binding sites, indicating that this bound ion prevents the rapid, complete loss of N-lobe structure. This small, folded region may explain the reduced translocation through Sec61 observed for CaM when Ca^{2+} is in solution, as described below (**Figure S6**).

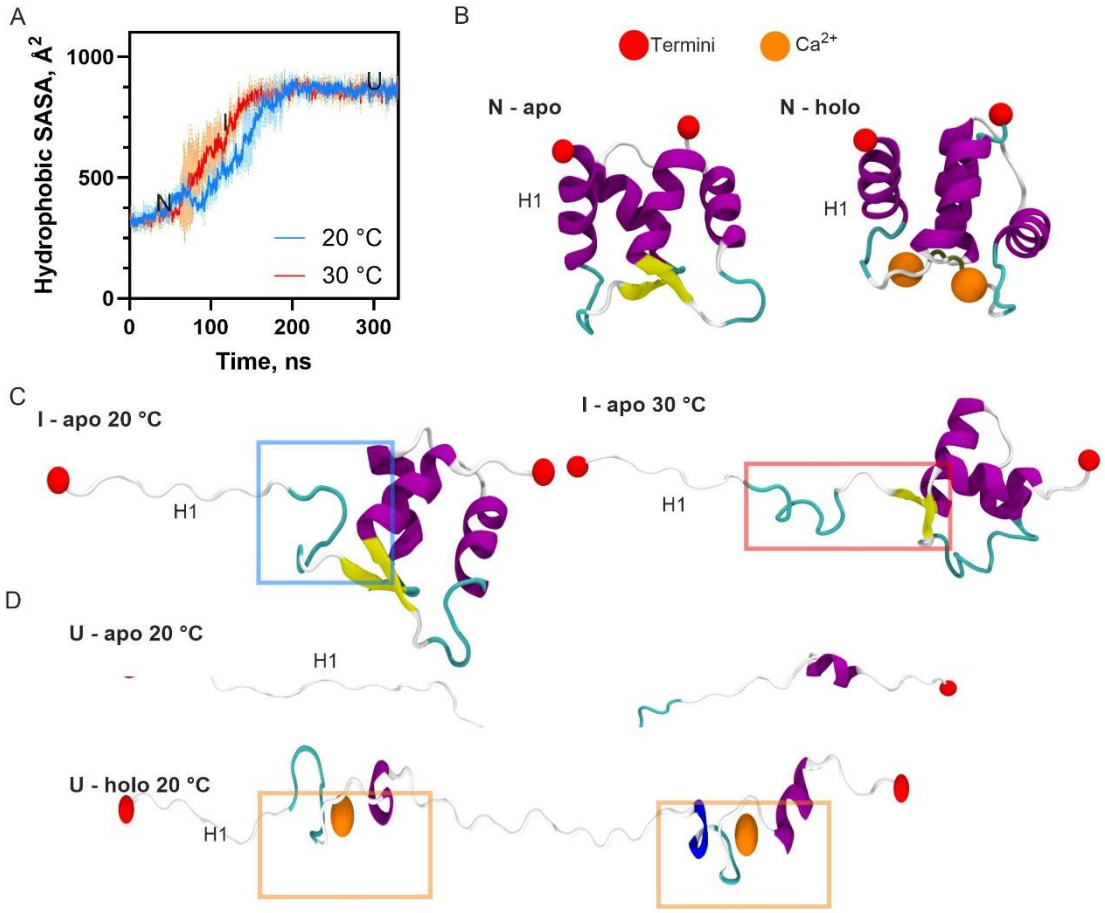


Figure 10. Effect of temperature and presence of Ca^{+2} on the mechanical unfolding of the N-terminus of CaM through steered molecular dynamics (SMD). Six simulations per condition were carried out for the unfolding of calmodulin at different temperatures and Ca^{2+} coordination states. **(A)** Solvent accessible surface area (SASA) of hydrophobic residues at helix H1 of apo-CaM at different temperatures (mean ± SD of six replicas). The trace shows three states: folded (N), H1 unfolding (I), and unfolded (U). **(B)** Cartoon representation of structures at the beginning of pulling for apo-CaM (PDB 1CFD) and holo-CaM (PDB 1CLL). **(C)** Structure of the H1-unfolded intermediate at 20 and 30 °C. The region containing the most hydrophobic contacts is highlighted for each representation. **(D)** Comparison between the final structure obtained for apo and holo CaM at 20 °C. The site surrounding the Ca^{2+} binding residues is highlighted.

3.2.- Chimera proteins can be translocated i*n vitro* by using a microsome-based assay and visualized by non-radioactive means

To perform an ER translocation assay, we prepared microsomes as described above and confirmed the components of post-translational translocation by Western blot (**Figure S2**).

To confirm microsome function and validate our experimental setup, we performed a translocation protease protection assay using purified recombinant ppαF for 1 hour at 20 °C. Traditionally, the translocation assays were performed using radiolabeled substrate synthesized *in vitro*. Here, we adapted and optimized the translocation assays without using radioactivity. We initially compared both methods and, as shown in **Figure 11**, autoradiography and immunoblotting showed similar percentages (no glycosylated, 20-24%) of translocation of the non- glycosylated 19 kDa ppαF band. Autoradiography also revealed the glycosylated ppαF species, but only after longer exposures in the Western blot analysis (**Figure S7**). As expected, this band is most intense in lanes containing only ppαF and microsomes (lanes 1 in **Figure 11A** and **Figure 11B**), as only translocated protein would be glycosylated. Successful translocation is further supported by the presence of a faint, lower-weight band (17 kDa) attributed to pαF, the product that has lost the signal sequence domain during translocation (Lecker et al., 1989).

Under microsomal protection from protease conditions (**Figure 11 A** and **B**, lane 2), band intensities decreased with respect to total protein added in the assay in the absence of proteases, indicating that microsomes protected the translocated proteins (**Figure 11 A** and **B**, lane 1). In contrast, when the microsomes were treated by the addition of detergent (TX-100), the protection was lost, and the translocated as well as non-translocated proteins were degraded (**Figure 11A** and **B**, lane 3), providing a value to exactly quantify the translocated proteins protected by microsomes (Lyman & Schekman, 1997). This amount was calculated as 23% visualized in the radioactivity assays and 25% in the Western blot

analysis. In both cases, the calculation excludes glycosylated bands. These results indicate that a non-radioactive protection assay works as well as the traditional assay.

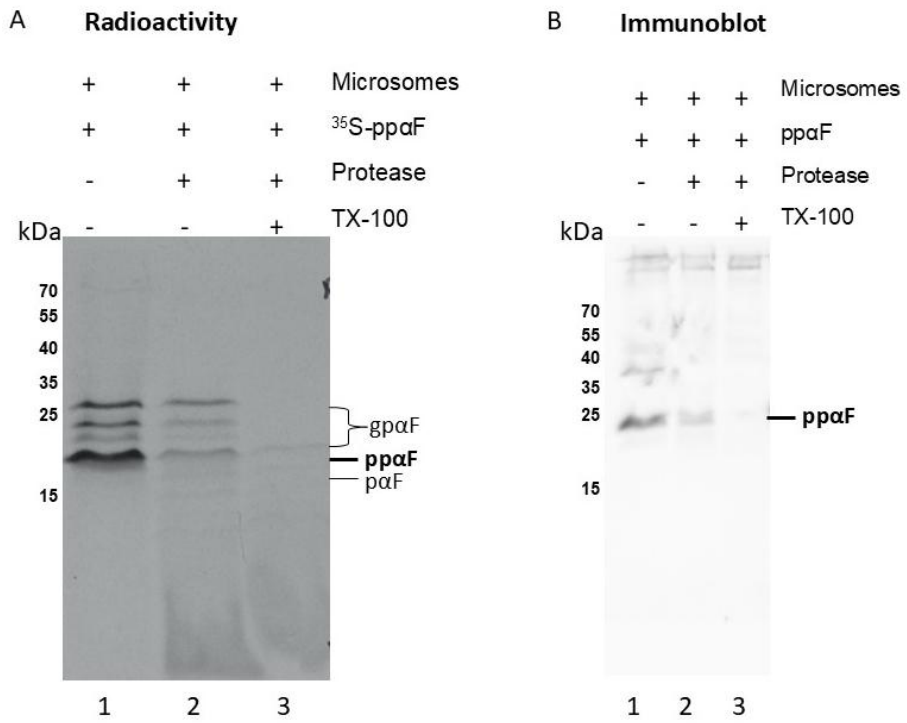


Figure 11. Prepro-α-Factor (ppαF) translocation assay visualized by radioactivity and Western blotting. Protection assays with purified microsomes and either radioactive or non-radioactive labeled ppαF were performed for 1 hour at 20 °C, as per "Materials and Methods". **(A)** Translocation of radioactive prepro-α-Factor visualized by a protease protection assay followed by autoradiography. **(B)** Translocation of purified recombinant prepro-α-Factor, visualized by a protease protection assay followed by Western blot analysis with an anti-ppαF. **(A)** and **(B)** Lane 1 – Total input: total protein in translocation assay; Lane 2 – protection assay, translocation assay treated with protease; Lane 3 – control, translocation assay treated with proteinase K in the presence of detergent. In both A and B, the translocated ppαF, glycosylated pro-α-factor (gpαF), and pro-α-factor (pαF) are protected from protease digestion by intact membranes (lane 2), but not when the membranes are dissolved by the detergent Triton (TX-100, lane 3). After the translocation assay, with or without protease treatment, we resolved proteins by SDS-PAGE at 12.5%. In A, the autoradiography was exposed for 16 h; in B, the SDS-PAGE was transferred to a nitrocellulose membrane, blocked, and incubated with anti-ppαF (16 h, diluted 1:10,000 at RT), followed by anti-rabbit-HRP-conjugated antibody (diluted 1:3000).

3.3.- Kinetics of chimera substrate translocation into microsomes determined by protease protection assays.

After validating the chimera's translocation assay to microsomes by Western blot, we characterized the translocation kinetics of Sec61 substrates. We first studied the translocation of a chimera containing two unfolded Titin-I27 mutant domains, a positive control for translocation as a fully unfolded construct. We designed it to measure the maximum translocation speed in this system, as this construct requires zero unfolding force to enter microsomes via the Sec61 channel. As reported in the literature, the translocation reaction plateaus at 1 h (Brodsky et al., 1995; Brodsky & Schekman, 1993). We performed these studies multiple times between 0 and 60 minutes at 20 °C to determine translocation rate and efficiency.

As shown in **Figure 12A**, Western blot analysis revealed the Titin-I27 mutant chimera band at ~28 kDa. A slightly smaller fraction also appeared at ~25 kDa, even in the absence of microsomes (**Figure S4**). Mass spectrometry identified this lower-migrating band as the unfolded Titin I27 mutant chimera lacking the signal sequence. The ~28 kDa band of the unfolded Titin I27 mutant chimera under protection assay conditions (i.e., microsomes + protease) reflects successful translocation into microsomes. This corroborates that the 25 kDa band cannot translocate because it lacks a signal sequence. The intensity of this protected band (28 kDa) increases over time, indicating the accumulation of the translocated chimera inside microsomes in the protease protection assay. In the presence of the protease (Tryp or PK) and Triton X-100 (TX-100), the ~28 kDa band disappears, indicating that most of the chimera protein has been degraded, including the translocated fraction. We used the western blot results to estimate the rate of unfolded Titin I27 mutant chimera translocation by measuring band intensities over time (see Materials and Methods). Quantification of band intensity over time showed a translocation rate of (0.61 ± 0.11)% per minute at 20 °C (**Figure 11B, Table 1**). These results confirm the translocation capacity of chimera constructs and provide a positive control for subsequent kinetic studies.

We then analyzed the translocation kinetics of the CaM chimera that exhibits a low unfolding force (~7 pN) (Goldman et al., 2015). CaM chimera protein (35 kDa band, bottom gel, **Figure 12A**) was observed in the total input condition. However, after protease treatment, we could only detect a minimal protected fraction after 60 minutes of the translocation reaction; therefore, we extended the incubation to 120 minutes (**Figure 12A**). The translocation rate determined by the longest incubation time was (0.03 ± 0.01)% per minute (**Table 1**). This low rate indicates that substrate unfolding is rate-limiting during post-translational translocation, as the unfolded Titin I27 mutant chimera positive control translocated faster, as previously reported *in vivo* (Bustamante et al., 2004).

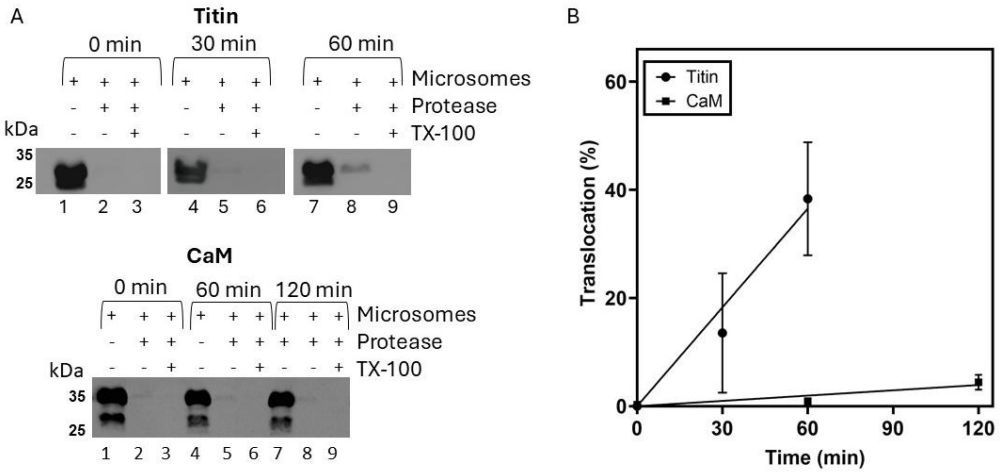


Figure 12. Translocation kinetics of chimera proteins. **(A)** Western blot images of translocation protection assays of unfolded Titin I27 mutant and CaM chimera. We incubated reactions at 20 °C and stopped them at the indicated time points. The running order of conditions was maintained as follows (left to right): total input (translocated or not), protection assay (translocation treated with protease), and microsome solubilization control (translocation treated with protease and detergent). We used anti-Titin (1:5,000) and anti-CaM (1:3,000) antibodies. **(B)** Percentage of translocation plotted as a function of time (min) for Titin and CaM chimeras, shown as mean (points) and SEM values (error bars) with a linear regression fit.

Finally, to test substrate translocation with high mechanical stability, we analyzed the Top7 chimera, which exhibits a high unfolding force of ~20 pN (**Figure 7A**). Although the expected 24.5 kDa band was clearly detected in the total input condition (that is, incubated with microsomes alone), no protected fraction was observed at any time point

up to 120 minutes at 20 °C Table 1; (**Figure S8**). This serves as a negative control for the protection assay results, showing that substrates with unfolding forces of 20 pN or higher cannot be mechanically unfolded or translocated by BiP in this *in vitro* system.

Temperature	Translocation Rate (% per minute)			
	Titin	CaM	CaM + EGTA	Top7
20°C	0.61 ± 0.11	0.03 ± 0.01	0.03 ± 0.01	0
30°C	1.03 ± 0.04	0.05 ± 0.01	0.08 ± 0.01	0.02 ± 0.01

Table 1. Mean and SD values of chimera translocation rates shown in % of translocation per minute. For 20 °C, we plotted translocation percentages from multiple replicates as a function of time (minutes) and fit them with linear regression. We obtained the translocation rate from the slope. The values are reported here with error margins. At 30 °C, we divided maximum translocation values by 60 min for the Titin chimera and by 120 min for the CaM and Top7 chimeras to obtain a percentage-per-minute value.

3.4.- Temperature and protein structure stability effects on translocation

To further elucidate how BiP mediates translocation, we evaluated how thermal energy influences substrate structural stability and translocation efficiency. As shown in **Figure 13A-B** and **Table 2**, there was no significant difference in the maximum translocation of the fully unfolded Titin I27 mutant chimeric increasing the temperature from 20 °C to 30 °C ((38.35 ± 10.44)% at 20 °C vs. (61.77 ± 4.01)% at 30 °C; $p = 0.238$). There was also no significant difference in CaM chimera ((4.15 ± 1.61)% at 20 °C vs. (5.67 ± 2.02)% at 30 °C; $p = 0.660$). Similarly, at high unfolding force, the Top7 chimera showed a minor translocation level after 120 minutes at 30 °C ((2.02 ± 0.77)%; $p = 0.114$). However, this was not significantly different from the zero-translocation estimate at 20 °C (**Table 2**).

These results prompted us to investigate whether other factors, such as calcium binding, could influence BiP-mediated translocation by modulating CaM stability.

Calcium binding stabilizes the calmodulin (CaM) structure, with the apo and calcium-bound states having distinct structures and surface properties (Finn et al., 1995; Zhang et al., 1995). Although CaM chimeras were purified in calcium-free conditions, isolated yeast microsomes retain endogenous calcium reserves in their lumen (Mayinger & Meyer, 1993). This favors the holo-CaM conformation, especially considering that Ca^{2+} binding negatively modulates translocation efficiency by interacting with the signal sequence (Shao & Hegde, 2011).

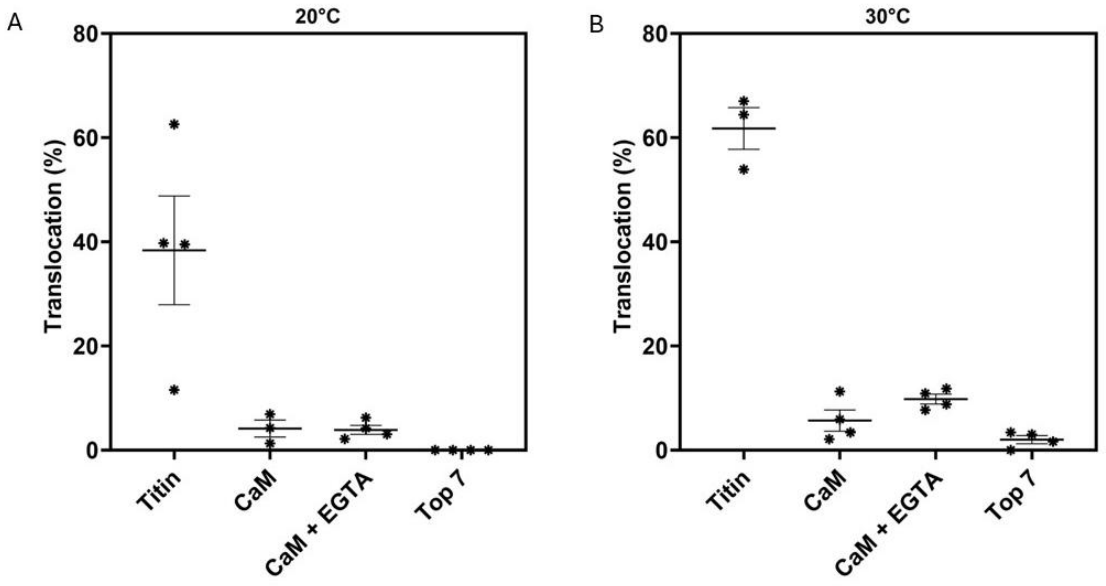


Figure 13. Maximum translocation of chimeras at different temperatures and conditions. Percentages of translocation observed after 2 hours of reaction time at **(A)** 20 °C and **(B)** 30 °C for Titin, CaM, and Top 7 chimeras are shown as scatter plots displaying mean and SD values. Translocation levels of CaM studies in the presence of EGTA at both temperatures are also shown. 20 °C N-values: Titin = 3, CaM = 5, CaM + EGTA = 5, Top 7 = 3. 30 °C N-values: Titin = 4, CaM = 6, CaM + EGTA = 9, Top 7 = 4.

Accordingly, we evaluated the effect of the calcium chelator EGTA to determine whether reducing substrate stability facilitates BiP-mediated import. At 20 °C, EGTA addition did not significantly affect total translocation (3.89 ± 0.87)% as shown in **Table 2**. However, at 30 °C, chelation of calcium by EGTA significantly increased the maximum translocation of CaM chimera to (9.80 ± 0.94)% with p = 0.015 (**Table 2**), with an

increased translocation rate to (0.08 ± 0.01)%/min (**Table 1**). This maximum translocation value also differs significantly from that of the CaM chimera in the absence of EGTA at 30° and from the Titin and Top7 constructs (**Table 2**), indicating that structure stabilization could prevent translocation by requiring extra force to unfold.

Chimera	% (20°C)	% (30°C)	P-Value
Titin	38.35 ± 10.44	61.77 ± 4.01	0.238
CaM	4.15 ± 1.61	5.67 ± 2.02	0.660
CaM+EGTA	3.89 ± 0.87	9.80 ± 0.94	0.015*
Top7	0	2.02 ± 0.77	0.114

Table 2. Mean, SD, and P-values of maximum translocation level percentages at 20 °C and 30 °C. Maximum translocation levels (after 1 hour for Titin and 2 hours for CaM and Top7) were measured for each chimera at 20 °C and 30 °C. We performed t-tests to compare outcomes across chimera studies at different temperatures. Statistical significances of * $p < 0.05$, ** $p < 0.01$, *** $p < 0.001$ are shown.

3.5. The kinetic rates of post-translational translocation are energy-dependent

To study the energy dependence of post-translational translocation in our *in vitro* system, we evaluated the translocation rate without exogenous ATP. The absence of ATP reduced the translocation rate to 8–10% after 60 min, 4-5 times less when compared to 38% observed in the presence of ATP (**Figure 14**). These results were similar to the translocation efficiency observed in microsomes from the Sec63 A179T mutant, which disrupts interaction with BiP (Misselwitz et al., 1999). At the restrictive temperature (37 °C, at which the yeast is not viable with the mutant; see **Figure 5**), this strain showed very low translocation (10.2% with ATP and 1% without ATP) at 60 min (**Figure 14 A** and **B**), consistent with literature reports of minimal translocation over time for this mutant (Rothblatt et al., 1989). Therefore, our results support the control and establish that continuous ATP turnover mediated by a functional BiP–Sec63 coupling is strictly required

for efficient forward translocation. The Brownian ratchet mechanism suggests that polypeptide movement occurs because the protein translocates by Brownian motion.

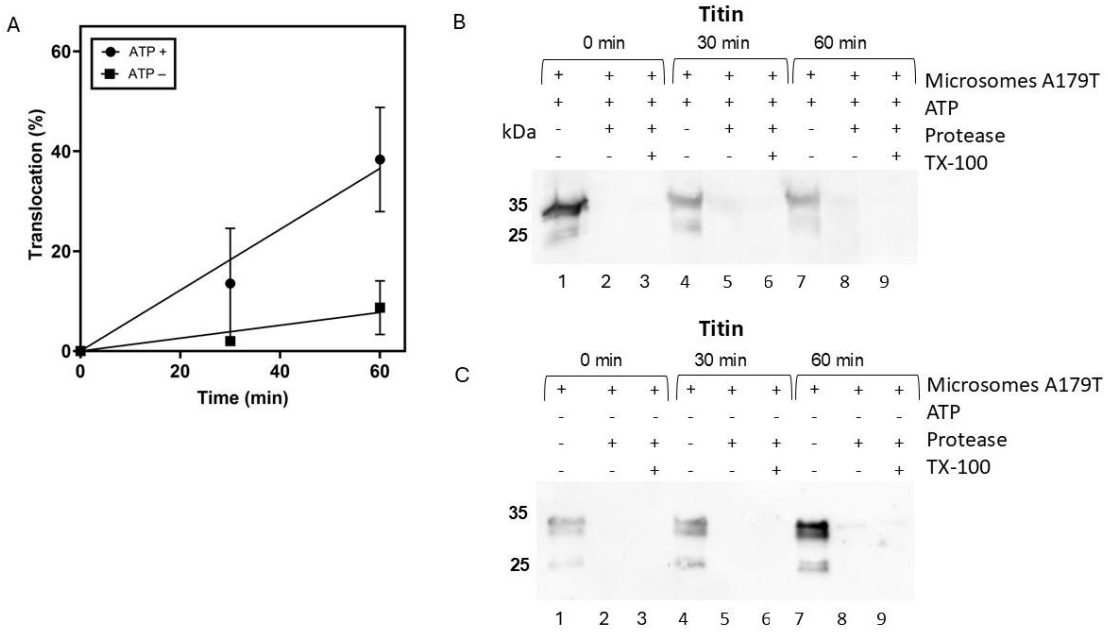


Figure 14. Translocation of the unfolded Titin I27 mutant chimera into microsomes is ATP-dependent and requires functional Sec63-BiP interaction. (A) Quantification of Titin I27 mutant chimera translocation efficiency into WT RSY1255 microsomes over time (0, 30, and 60 min) in the presence (ATP+, circles) or absence (ATP−, squares) of ATP. Data represent mean ± SEM (n=3). **(B)** Translocation assay using a Sec63 (A179T) mutant microsome, which disrupts the interaction between BiP and Sec63 J-domain in the presence of ATP. Lane 1, 4, and 7: total input; Lane 2, 5, and 8: protection assay. Lanes 3, 6, and 9: protease and TX-100 conditions. **(C)** Translocation assay using a Sec63 (A179T) mutant microsome, which disrupts the interaction between BiP and Sec63 J-domain in the absence of ATP. Lane 1, 4, and 7: total input; Lane 2, 5, and 8: protection assay. Lanes 3, 6, and 9: protease and TX-100 conditions.

3.6.- The output power of BiP is closer to that of ratchet molecular motors than to power stroke

Using Optical Tweezers force-ramp assays, we determined that Top7 unfolds at 20 pN when pulling at 100 nm/s at both 20 and 30 °C. These unfolding forces can be used to estimate the work BiP must apply to unfold and translocate folded proteins *in vivo*, providing new insights into the coupling of these two main physical processes: unfolding and translocation. Work can be calculated by multiplying the unfolding force values by

the molecular motor step size (Materials and Methods (Cecconi et al., 2008)).

In the case of Top7, the work performed by BiP to unfold and translocate this protein in an efficient manner must fall within the range of 20 pN*nm or 5 k_BT (using a step size of 1 nm, Marcinowski et al., 2011) and 48 pN*nm or 12 k_BT (using a step size of 2.4 nm, Yamano et al., 2008). Both values exceed the 3 k_BT set by the thermal bath, suggesting that Top7 translocation must be driven by factors beyond Brownian motion. However, because we observed no Top7 translocation in our assay, we propose that, in this system, BiP cannot act as an active molecular motor or mechanically induce translocation by exerting forces on the protein.

In the case of CaM, we estimated a work of 7-16.8 pN · nm (or 1.7-4 k_BT, respectively). The maximum level of work proposed to complete translocation is slightly above 3 k_BT; however, very small amounts of CaM translocation were detected, suggesting that the force and work actively applied by BiP must be zero, in line with the ratchet mode of action. In addition, these results support the idea that here, the BiP step size may be closer to 2.4 nm, as reported by Yamano et al (2008). using mitochondrial HSP70 (Yamano et al., 2008). If the requisite energy for translocation were less than 3 k_BT (as would be the case if the step size were 1 nm), the surrounding fluctuations would promote translocation and allow it to be observed. Given that 3 k_BT is equivalent to 12.34 pN/nm of work and the chimera's unfolding force is 7 pN, the minimum step size must be at least 1.7 nm.

Force-ramp assays show that higher-force unfolding events occur at higher pulling velocities, as unfolding force peaks depend on the pulling speed at which the force-ramp assay is performed (Dudko et al., 2008). However, CaM exhibits an unfolding-refolding equilibrium at 7 pN (Goldman et al., 2015), indicating that regardless of the speed at which a molecular motor such as BiP pulls the construct, the unfolding force remains at 7 pN. Thus, by comparing the unfolding kinetics of CaM at 7 pN with the translocation rate, we can gauge whether these events occur with a similar order of magnitude.

In addition to the mechanical work performed by the molecular motor, the translocation kinetics assay results also allow an estimation of the average mechanical output power ($P = F\ x\ v$) developed during translocation. The unfolded Titin I27 mutant chimera is 282 amino acids long, or 95.9 nm, assuming one amino acid corresponds to 0.34 nm (Ainavarapu et al., 2007). Consequently, with a translocation rate of 0.61%/min obtained at 20 °C (Table 1), and taking into account the number of channels by vesicle (Wang et al., 2017; West et al., 2011) that we have in our experiment and the concentration of BiP calculated for us (14 μM inside the microsomes), the average speed for the complete translocation of the whole protein is approximately 1 nm/sec. This is similar to values previously reported (Liebermeister et al., 2001). Therefore, if BiP exerts a force of 7 pN and the average mechanical power developed by BiP is 7 pN · nm/sec or 1.7 kBT/sec (**see Table 3**). This result is several orders of magnitude smaller than the average power developed by power-stroke motors such as kinesin (P ~ 1400 kBT/sec), but comparable with ratchet molecular motors like RNA polymerase (P ~ 16.5 kBT/sec) (Bustamante et al., 2004). Therefore, the mechanical output power of BiP is more consistent with a ratchet molecular motor than with a power stroke.

Chimera	Unfolding force (pN)	Step Size (nm)	Work (pN*nm)	Work (k_BT)	Output power (pN*nm/s)	Output power (k_BT/s)
Titin	0	1 - 2.4	---	---	---	---
CaM	7	1 - 2.4	7 - 16.8	1.7 - 4.1	7	1.7
Top7	20	1 - 2.4	20 - 48	4.9 - 11.7	20	4.9

Table 3. Translocation requirements and parameters for each protein construct. We provide a range of work required for the translocation of each chimera based on the range of BiP molecular motor step size suggested from previous findings (Marcinowski et al., 2011). Output power uses the experimentally derived speed of translocation in this system as 1 nm/sec.

Chapter 4

Discussion

Our results from a microsome-based protease protection assay quantifying the translocation kinetics of chimeric substrates with defined unfolding forces are consistent with the idea that BiP does not function as a high-force motor to enhance ER membrane translocation. Instead, our findings show that substrate unfolding limits BiP-mediated translocation, so BiP cannot exert sufficient force to unfold protein domains such as CaM and Top7.

We tested the BiP-dependent translocation machinery using chimeric substrates with different unfolding forces (Top7, 20 pN; and CaM, 7 pN; Goldman et al., (2015)). We observed the highest translocation efficiency with the fully unfolded Titin I27 mutant chimera, which remained in a denatured conformation throughout the assay. These robust translocation results validate the microsomal system's functional integrity without requiring mechanical unfolding. In contrast, substrates containing a folded domain showed markedly reduced translocation efficiency, with the strongest impairment for the mechanically more stable Top7 substrate and intermediate reduction for CaM. Thus, translocation efficiency decreases with increasing folding stability, suggesting that folded domains hinder import through the Sec61 channel. This finding is consistent with previous studies showing that stabilization of folded domains can inhibit ER translocation both *in vitro* and in living cells (Conti et al., 2014; Kida et al., 2005).

Our studies of translocation rates provide key insights into BiP's mechanochemical mechanism. If the translocation rate significantly exceeds the unfolding rate of a substrate chimeric protein, it implies that external mechanical forces are acting

on the substrate. Therefore, the unfolding energy barrier exceeds the thermal contribution (3 kBT). Conversely, similar or slower translocation rates relative to unfolding rates indicate an unassisted process in which substrate unfolding must occur independently before import, and BiP can trigger translocation. We estimated the unfolding rate of CaM to be 1 s-1 at 7 pN using optical tweezers data (Goldman et al., 2015). CaM translocates at a significantly slower rate than it unfolds. Therefore, this result shows that no force is applied to promote substrate unfolding and pull it through the Sec61 channel, suggesting that BiP acts as a Brownian ratchet molecular motor rather than a pulling motor.

The maximum translocation efficiency observed for the fully unfolded Titin chimera was approximately 55–60% after 60 minutes. This value is similar to post-translational translocation efficiencies reported in the literature using yeast microsomes. The reported range is between 40-60% for substrates such as ppαF historically studied for translocation assays (Brodsky et al., 1993; Rothblatt et al., 1989). The fact that a completely unfolded substrate does not reach 100% import is a well-established characteristic of *in vitro* microsomal systems, reflecting inherent physical and functional constraints such as non-translocating vesicle orientations, stochastic inactivation of Sec61 translocons, or progressive ATP depletion over extended incubation times.

Therefore, achieving ~60% translocation with our positive control validates the structural and functional integrity of our isolated yeast microsomes, confirming that the setup was fully competent for transport. Consequently, the drastic reduction in translocation efficiency observed for folded substrates, such as CaM (~4–9%) and Top7 (~0%), can be definitively attributed to the energy barrier imposed by substrate unfolding rather than to impaired microsomal functionality.

Accordingly, mechanical work and output power calculations suggest that the energy provided by either BiP or environmental contributions is insufficient to facilitate unfolding and translocation of Top7 and CaM protein constructs through microsomal membranes. These findings support the notion that translocation is driven by Brownian

motion, biased by BiP's ratchet mechanism. Indeed, the results indicate that spontaneous unfolding occurs independently and prior to movement through the channel. BiP exploits this movement rather than actively driving unfolding through force. Therefore, conformational changes and ATP hydrolysis by BiP do not directly contribute energy to the translocation system, as observed in power-stroke motors. Instead, ATP hydrolysis occurs only because of BiP's distinct binding affinity for its substrate. It is important to recall that the estimation of BiP's mechanical output power is based on the assumption of complete availability of the components of microsomes involved in translocation, such as the Sec61 channel and BiP, and that the number of BiP proteins is equal to or greater than the number of proteins to be translocated.

Although we estimated that the BiP concentration in the microsomes is in the micromolar range (**Figure S1**), which is at the lower end of those reported *in vivo* (Lai et al., 2010; Zimmermann & Lang, 2020), we calculated that we have a 100-fold excess of BiP inside the microsome relative to the channels. Thus, the translocation speed estimated from the kinetic assays is similar to the translocation speed observed *in vivo* (Liebermeister et al., 2001). In summary, our results suggest that the average power developed by BiP may be approximately 1-10 kBT/sec, placing BiP at the lower end of ratchet molecular motors.

Given the greater supply of thermal energy at higher temperatures (e.g., 30 °C) (Van Holde et al., 2006), we also investigated how increased temperature would facilitate spontaneous protein unfolding and translocation. Previous studies have described how temperature modulates mechanical unfolding and refolding in the presence of BiP (Rivera, Burgos-Bravo, et al., 2023; Rivera, Mjaavatten, et al., 2023). Notably, increasing the temperature from 20 °C to 30 °C did not significantly enhance translocation efficiency (Rivera, Mjaavatten, et al., 2023).

This observation indicates that the thermal fluctuations presumed to drive translocation do not significantly influence the efficiency of this process, either by

promoting spontaneous unfolding or by ensuring adequate Brownian motion. Given that ATP hydrolysis is highly regulated by temperature (Rivera, Burgos-Bravo, et al., 2023), the absence of a temperature effect on protein translocation also indicates that ATP hydrolysis does not contribute to the translocation process. These results correlate with the previous observation that BiP binds similarly to the substrate across a wide range of temperatures (Rivera, Burgos-Bravo, et al., 2023).

Interestingly, temperature significantly affected translocation efficiency when calcium chelation destabilized the CaM structure (Junker et al., 2009; Stigler & Rief, 2012). At very low calcium concentrations, CaM assumes a flexible apo structure with large conformational differences compared to the more stable calcium-bound holo state (Finn et al., 1995). Single-molecule force spectroscopy experiments also show that lowering the calcium concentration from 10 mM to 100 μM decreases the free energy of all states along the unfolding pathway (Stigler et al., 2011). Moreover, low calcium concentrations (100 μM) reduce the unfolding forces drastically to 5 pN, while the absence of calcium resulted in unfolding forces < 3 pN (Stigler & Rief, 2012). Consistently, we found that CaM in the absence of calcium is more prone to be translocated mainly at higher temperatures.

To understand how BiP could interact with folded substrates during import, steered molecular dynamics (SMD) simulations provided crucial atomistic information on the mechanical unfolding pathway of apo-CaM. At 30 °C, Helix 1 (residues 7–21) at the N-terminus undergoes local thermal destabilization, losing tertiary contacts and exposing hydrophobic residues significantly earlier than at 20 °C. This local unwinding at the N-terminus is mechanistically critical: it demonstrates that global mechanical unfolding of the entire domain is not required before channel engagement. Instead, local thermal fluctuations could allow the N-terminal segment to spontaneously unfold, exposing an extended polypeptide chain that BiP can sequentially trap on the luminal side of the Sec61 channel via a Brownian ratchet mechanism.

In establishing a reliable non-radioactive protease protection assay, methodological optimization was crucial to eliminate potential experimental artifacts, particularly during detergent-mediated membrane solubilization. Fully or partially unfolded chimeric proteins, such as the Titin construct, expose extensive hydrophobic regions that render them prone to non-specific aggregation in solutions. Initial co-incubation of Triton X-100 and Proteinase K over extended timeframes (e.g., 120 min) resulted in substrate aggregation, which sterically hindered proteolysis and generated false-positive protected bands in the total digestion controls.

To address this limitation, we refined the digestion protocol by restricting Triton X-100 exposure (0.3% v/v) to the final 10 minutes of the 30-minute Proteinase K incubation. This addition enabled rapid, complete microsomal membrane disruption without inducing hydrophobic substrate aggregation, ensuring full degradation of non-translocated proteins under control conditions. This technical refinement guaranteed high quantitative accuracy across all kinetic time points, confirming that protected bands represented true luminal translocation events.

Our experimental data in the presence of EGTA strongly support this model. Chelation of calcium forces CaM into its highly flexible apo-state, drastically lowering its unfolding force (< 3–5 pN). When combined with elevated temperature (30 °C), which enhances local thermal fluctuations, CaM translocation efficiency increased significantly to ~9.8%. Together, these results confirm that BiP does not actively exert a high mechanical force to unfold substrates (as predicted by a power stroke model); rather, it relies on thermal energy to destabilize fragile structural elements, taking advantage of local unfolded intermediates to bias unidirectional translocation.

Thus, these results suggest that when protein stability and unfolding forces are reduced, BiP requires less work during translocation, supporting the model in which BiP behaves as a ratchet motor. Considering the unfolding forces reported at 100 or 0 μM calcium concentration, the work required of BiP to unfold and translocate CaM *in vivo*

must be around 5 pN*nm (2.9 kBT) and 7.2 pN*nm (1.8 kBT), respectively. Because these values are lower than thermal energy, we could detect translocation of destabilized CaM protein; however, only at slow rates. The latter is consistent with the proposed statement that BiP does not apply additional forces to unfold and thus translocate the CaM protein, as in ratchet activity. It is important to note that CaM destabilization enhances translocation efficiency only when the temperature is elevated concomitantly. This indicates that reduced work requirements (i.e., due to protein destabilization) are insufficient to enable BiP-mediated protein translocation, and that additional thermal energy from the surrounding environment is necessary (Dudko et al., 2008).

Our results suggest that the translocation process mediated by BiP starts only after the spontaneous unfolding of the protein (i.e., in the absence of mechanical forces). For CaM, spontaneous unfolding occurs on a time scale of 1 second (Goldman et al., 2015), while for Top7 it is around 100 seconds (Li et al., 2021). We obtained these unfolding rates by linearly extrapolating to zero force in lifetime vs. force plots. However, our data suggest a different regime in which waiting times (i.e., for spontaneous unfolding) can reach up to 104 sec, several orders of magnitude larger than the value obtained by extrapolation under almost-zero-force conditions (Goldman et al., 2015).

Additionally, single-molecule analysis has revealed protein folding and unfolding as a superposition of two force-independent and force-dependent processes, dominant at low and high force, respectively, with a turnover between them (Best et al., 2008). Consequently, proteins are expected to fold and unfold at different rates depending on the effective force applied to them (Graham & Best, 2011; Rico-Pasto et al., 2022). In BiP-mediated translocation, our results indicate that translocating proteins experience relatively modest forces, leading to unfolding rates significantly lower than previously reported. This, in turn, slows the entire translocation process (Best et al., 2008). This interpretation is consistent with our results. The proteins studied here show markedly different unfolding rates at near-zero force, with Titin the fastest and Top7 the slowest. Moreover, these findings may provide valuable insights for developing new methods to

estimate protein unfolding rates under near-zero-force conditions.

Finally, the entropic pulling model couples the two canonical motor types, power-stroke and ratchet, and Brownian motion still plays a central role. As such, the substrate will unfold both spontaneously and when pulled across the membrane. Our results show that the force exerted by BiP is lower than the 10–15 pN proposed by this mechanism.

Chapter 5

Conclusions

This doctoral research addressed the biophysical and mechanochemical characterization of the chaperone protein BiP to elucidate its mechanism of action as a molecular motor during post-translational protein translocation through the Sec61 channel in Saccharomyces cerevisiae. This allowed us to reach the following main conclusions:

We developed an *in vitro* microsome-based system to estimate the force that BiP can exert during protein translocation, using protease protection assays. We also validated the functionality of microsomes obtained using two different methods with ppαF, a substrate widely used in post-translational protein translocation studies. Translocation rates obtained with the Titin chimera allowed us to validate our experimental model and, over time, evaluate the translocation rates of low- and high-force chimeric proteins.

Translocation efficiency and speed depend on the substrate's structural stability. While the fully unfolded chimera (positive control, mutant Titin I27, 0 pN) achieved translocation efficiencies of ~38% with a rate of 0.61%/min (20 °C), chimeras with folded domains showed a drastic restriction in transport. The Top7 chimera (~20 pN) exhibited a null rate (0%/min), while calmodulin (CaM, ~7 pN) showed markedly low translocation (0.03%/min), confirming that BiP lacks the mechanical capacity to actively unfold structured domains at the channel entrance.

Our findings demonstrate that BiP cannot actively unfold the protein substrate and therefore requires the protein to be pre-unfolded. Thus, we propose that BiP acts as a passive ratchet motor, in which ATP hydrolysis provides the specificity and affinity that allow BiP to interact with the protein substrate, rather than supplying energy to exert a

force greater than that of the heat bath and actively translocate the protein. This mechanism involves Brownian diffusion of unfolded proteins, driven by thermal fluctuations (Bustamante et al., 2004). BiP binding then rectifies the directionality of polypeptide translocation within the microsome.

Calculations of mechanical work ($W=F\times D$) and mechanical power output ($P=F\times v$) support the passive ratchet nature of the mechanism. The power generated by BiP during CaM translocation was estimated at 7 pN·nm/s (1.7 k_BT/s), a value several orders of magnitude lower than that of typical high-power motors reported in the literature (such as kinesin, $P \approx 1400\ k_BT$/s) (Bustamante et al., 2004).

This experimental strategy will allow us to better understand other molecular motors that could be integrated into the microsome system, such as the mitochondrial chaperones Hsp70 and the chloroplast chaperones Hsp93, whose mechanisms of action have not yet been determined. As future projections, based on the findings and methodological tools, we will continue with the comparative analysis of translocation kinetics using the transformed strains Sec63-Flag (wild-type) and the variant with a point mutation in the J domain (Sec63-Flag A179T). This mutation alters the stimulation of BiP ATPase activity without destroying the Sec62/Sec63 complex. Furthermore, we can compare the translocation rates over time of a glycosylated protein (ppaF) versus the non-glycosylated chimera Titin. This could be relevant for determining how much glycosylation contributes to the translocation rate.

Furthermore, the biophysical interaction between BiP and the Sec61 channel is projected to be quantitatively characterized. It is essential to clarify the nucleotide dependence of this complex by evaluating how ATP- or ADP-bound states modulate binding affinity, interaction kinetics (k_{on} and k_{off}), and complex stability. This aims to further explore the mechanochemical coupling between the stimulation of BiP ATPase activity mediated by the J domain of Sec63 and the conformational changes associated with this catalytic cycle.

References

Abraham, M. J., Murtola, T., Schulz, R., Páll, S., Smith, J. C., Hess, B., & Lindahl, E. (2015). GROMACS: High performance molecular simulations through multi-level parallelism from laptops to supercomputers. *SoftwareX*, *1–2*, 19–25. https://doi.org/10.1016/j.softx.2015.06.001

Ainavarapu, S. R. K., Brujić, J., Huang, H. H., Wiita, A. P., Lu, H., Li, L., Walther, K. A., Carrion-Vazquez, M., Li, H., & Fernandez, J. M. (2007). Contour Length and Refolding Rate of a Small Protein Controlled by Engineered Disulfide Bonds. *Biophysical Journal*, *92*(1), 225–233. https://doi.org/10.1529/biophysj.106.091561

Ast, T., Cohen, G., & Schuldiner, M. (2013). A Network of Cytosolic Factors Targets SRP-Independent Proteins to the Endoplasmic Reticulum. *Cell*, *152*(5), 1134–1145. https://doi.org/10.1016/j.cell.2013.02.003

Astumian, R. D. (1997). Thermodynamics and Kinetics of a Brownian Motor. *Science*, *276*(5314), Article 5314. https://doi.org/10.1126/science.276.5314.917

Best, R. B., Paci, E., Hummer, G., & Dudko, O. K. (2008). Pulling Direction as a Reaction Coordinate for the Mechanical Unfolding of Single Molecules. *The Journal of Physical Chemistry B*, *112*(19), 5968–5976. https://doi.org/10.1021/jp075955j

Blond-Elguindi, S. (1993). Affinity panning of a library of peptides displayed on bacteriophages reveals the binding specificity of BiP. *Cell*, *75*(4), 717–728. https://doi.org/10.1016/0092-8674(93)90492-9

Brodsky, J. L., Goeckeler, J., & Schekman, R. (1995). BiP and Sec63p are required for both co- and posttranslational protein translocation into the yeast endoplasmic reticulum. *Proceedings of the National Academy of Sciences*, *92*(21), Article 21.

https://doi.org/10.1073/pnas.92.21.9643

Brodsky, J. L., Hamamoto, S., Feldheim, D., & Schekman, R. (1993). Reconstitution of protein translocation from solubilized yeast membranes reveals topologically distinct roles for BiP and cytosolic Hsc70. *The Journal of Cell Biology*, *120*(1), Article 1. https://doi.org/10.1083/jcb.120.1.95

Brodsky, J. L., & Schekman, R. (1993). A Sec63p-BiP complex from yeast is required for protein translocation in a reconstituted proteoliposome. *The Journal of Cell Biology*, *123*(6), Article 6. https://doi.org/10.1083/jcb.123.6.1355

Bush, G. L., Tassin, A. M., Fridén, H., & Meyer, D. I. (1991). Secretion in yeast. Purification and in vitro translocation of chemical amounts of prepro-alpha-factor. *Journal of Biological Chemistry*, *266*(21), Article 21. https://doi.org/10.1016/S0021-9258(18)92773-0

Bustamante, C., Chemla, Y. R., Forde, N. R., & Izhaky, D. (2004). Mechanical Processes in Biochemistry. *Annual Review of Biochemistry*, *73*(1), Article 1. https://doi.org/10.1146/annurev.biochem.72.121801.161542

Cecconi, C., Shank, E. A., Dahlquist, F. W., Marqusee, S., & Bustamante, C. (2008). Protein-DNA chimeras for single molecule mechanical folding studies with the optical tweezers. *European Biophysics Journal*, *37*(6), 729–738. https://doi.org/10.1007/s00249-007-0247-y

Chattopadhyaya, R., Meador, W. E., Means, A. R., & Quiocho, F. A. (1992). Calmodulin structure refined at 1.7 Å resolution. *Journal of Molecular Biology*, *228*(4), 1177–1192. https://doi.org/10.1016/0022-2836(92)90324-D

Conti, B. J., Elferich, J., Yang, Z., Shinde, U., & Skach, W. R. (2014). Cotranslational folding inhibits translocation from within the ribosome–Sec61 translocon complex. *Nature Structural & Molecular Biology*, *21*(3), 228–235. https://doi.org/10.1038/nsmb.2779

Craig, E. A. (2018). Hsp70 at the membrane: Driving protein translocation. *BMC Biology*, *16*(1), 11. https://doi.org/10.1186/s12915-017-0474-3

De Los Rios, P., Ben-Zvi, A., Slutsky, O., Azem, A., & Goloubinoff, P. (2006). Hsp70 chaperones accelerate protein translocation and the unfolding of stable protein aggregates by entropic pulling. *Proceedings of the National Academy of Sciences*, *103*(16), 6166–6171. https://doi.org/10.1073/pnas.0510496103

de Lorenzo, S., Ribezzi-Crivellari, M., Arias-Gonzalez, J. R., Smith, S. B., & Ritort, F. (2015). A Temperature-Jump Optical Trap for Single-Molecule Manipulation. *Biophysical Journal*, *108*(12), Article 12. https://doi.org/10.1016/j.bpj.2015.05.017

Deshaies, R. J., Koch, B. D., Werner-Washburne, M., Craig, E. A., & Schekman, R. (1988). A subfamily of stress proteins facilitates translocation of secretory and mitochondrial precursor polypeptides. *Nature*, *332*(6167), 800–805. https://doi.org/10.1038/332800a0

Dill, J. (2012). *Struts, springs and crumple zones: Protein structures under force* [UC Berkeley]. https://escholarship.org/uc/item/69r5s9s3

Dudko, O. K., Hummer, G., & Szabo, A. (2008). Theory, analysis, and interpretation of single-molecule force spectroscopy experiments. *Proceedings of the National Academy of Sciences*, *105*(41), Article 41. https://doi.org/10.1073/pnas.0806085105

Eastman, P., Galvelis, R., Peláez, R. P., Abreu, C. R. A., Farr, S. E., Gallicchio, E., Gorenko, A., Henry, M. M., Hu, F., Huang, J., Krämer, A., Michel, J., Mitchell, J. A., Pande, V. S., Rodrigues, J. P., Rodriguez-Guerra, J., Simmonett, A. C., Singh, S., Swails, J., … Markland, T. E. (2024). OpenMM 8: Molecular Dynamics Simulation with Machine Learning Potentials. *The Journal of Physical Chemistry. B*, *128*(1), 109–116. https://doi.org/10.1021/acs.jpcb.3c06662

Feizi, A., Gatto, F., Uhlen, M., & Nielsen, J. (2017). Human protein secretory pathway genes are expressed in a tissue-specific pattern to match processing demands of the secretome. *Npj*

Systems Biology and Applications, *3*(1), 22. https://doi.org/10.1038/s41540-017-0021-4

Fernández, F. S., Trombetta, S. E., Hellman, U., & Parodi, A. J. (1994). Purification to homogeneity of UDP-glucose:glycoprotein glucosyltransferase from Schizosaccharomyces pombe and apparent absence of the enzyme fro Saccharomyces cerevisiae. *The Journal of Biological Chemistry*, *269*(48), 30701–30706.

Finn, B. E., Evenäs, J., Drakenberg, T., Waltho, J. P., Thulin, E., & Forsén, S. (1995). Calcium-induced structural changes and domain autonomy in calmodulin. *Nature Structural & Molecular Biology*, *2*(9), 777–783. https://doi.org/10.1038/nsb0995-777

Glick, B. S. (1995). Can Hsp70 proteins act as force-generating motors? *Cell*, *80*(1), Article 1. https://doi.org/10.1016/0092-8674(95)90444-1

Goldman, D. H., Kaiser, C. M., Milin, A., Righini, M., Tinoco, I., & Bustamante, C. (2015). Mechanical force releases nascent chain–mediated ribosome arrest in vitro and in vivo. *Science*, *348*(6233), 457–460. https://doi.org/10.1126/science.1261909

Graham, T. G. W., & Best, R. B. (2011). Force-Induced Change in Protein Unfolding Mechanism: Discrete or Continuous Switch? *The Journal of Physical Chemistry B*, *115*(6), 1546–1561. https://doi.org/10.1021/jp110738m

Greenfield, N. J. (2006). Using circular dichroism spectra to estimate protein secondary structure. *Nature Protocols*, *1*(6), 2876–2890. https://doi.org/10.1038/nprot.2006.202

Greiner, W., Neise, L., & Stöcker, H. (1995). *Thermodynamics and Statistical Mechanics*. Springer New York. https://doi.org/10.1007/978-1-4612-0827-3

Hansen, W., Garcia, P. D., & Walter, P. (1986). In vitro protein translocation across the yeast endoplasmic reticulum: ATP-dependent post-translational translocation of the prepro-α-factor. *Cell*, *45*(3), 397–406. https://doi.org/10.1016/0092-8674(86)90325-9

Itskanov, S., & Park, E. (2023). Mechanism of Protein Translocation by the Sec61 Translocon Complex. *Cold Spring Harbor Perspectives in Biology*, *15*(1), Article 1.

https://doi.org/10.1101/cshperspect.a041250

Junker, J. P., Ziegler, F., & Rief, M. (2009). Ligand-dependent equilibrium fluctuations of single calmodulin molecules. *Science*, *323*(5914), 633–637. https://doi.org/10.1126/science.1166191

Kida, Y., Mihara, K., & Sakaguchi, M. (2005). Translocation of a long amino-terminal domain through ER membrane by following signal-anchor sequence. *The EMBO Journal*, *24*(18), 3202–3213. https://doi.org/10.1038/sj.emboj.7600788

Kuhlman, B., Dantas, G., Ireton, G. C., Varani, G., Stoddard, B. L., & Baker, D. (2003). Design of a Novel Globular Protein Fold with Atomic-Level Accuracy. *Science*, *302*(5649), Article 5649. https://doi.org/10.1126/science.1089427

Lai, C. W., Aronson, D. E., & Snapp, E. L. (2010). BiP availability distinguishes states of homeostasis and stress in the endoplasmic reticulum of living cells. *Molecular Biology of the Cell*, *21*(12), 1909–1921. https://doi.org/10.1091/mbc.e09-12-1066

Lecker, S., Meyer, D., & Wickner, W. (1989). Export of prepro-alpha-factor from Escherichia coli. *The Journal of Biological Chemistry*, *264*(3), 1882–1886.

Li, J., Chen, G., Guo, Y., Wang, H., & Li, H. (2021). Single molecule force spectroscopy reveals the context dependent folding pathway of the C-terminal fragment of Top7. *Chemical Science*, *12*(8), 2876–2884. https://doi.org/10.1039/D0SC06344D

Liebermeister, W., Rapoport, T. A., & Heinrich, R. (2001). Ratcheting in post-translational protein translocation: A mathematical model11Edited by G. von Heijne. *Journal of Molecular Biology*, *305*(3), 643–656. https://doi.org/10.1006/jmbi.2000.4302

Lyman, S. K., & Schekman, R. (1995). Interaction between BiP and Sec63p is required for the completion of protein translocation into the ER of Saccharomyces cerevisiae. *The Journal of Cell Biology*, *131*(5), Article 5. https://doi.org/10.1083/jcb.131.5.1163

Lyman, S. K., & Schekman, R. (1997). Binding of Secretory Precursor Polypeptides to a

Translocon Subcomplex Is Regulated by BiP. *Cell*, *88*(1), Article 1. https://doi.org/10.1016/S0092-8674(00)81861-9

M. Alfaro-Valdés, H., Burgos-Bravo, F., Casanova-Morales, N., Quiroga-Roger, D., & A.M. Wilson, C. (2019). Mechanical Properties of Chaperone BiP, the Master Regulator of the Endoplasmic Reticulum. In A. Català (Ed.), *Endoplasmic Reticulum*. IntechOpen. https://doi.org/10.5772/intechopen.82080

Marcinowski, M., Höller, M., Feige, M. J., Baerend, D., Lamb, D. C., & Buchner, J. (2011). Substrate discrimination of the chaperone BiP by autonomous and cochaperone-regulated conformational transitions. *Nature Structural & Molecular Biology*, *18*(2), Article 2. https://doi.org/10.1038/nsmb.1970

Matlack, K. E. S., Misselwitz, B., Plath, K., & Rapoport, T. A. (1999). BiP Acts as a Molecular Ratchet during Posttranslational Transport of Prepro-α Factor across the ER Membrane. *Cell*, *97*(5), Article 5. https://doi.org/10.1016/S0092-8674(00)80767-9

Mayinger, P., & Meyer, D. I. (1993). An ATP transporter is required for protein translocation into the yeast endoplasmic reticulum. *The EMBO Journal*, *12*(2), 659–666. https://doi.org/10.1002/j.1460-2075.1993.tb05699.x

McCarty, J. S., Buchberger, A., Reinstein, J., & Bukau, B. (1995). The Role of ATP in the Functional Cycle of the DnaK Chaperone System. *Journal of Molecular Biology*, *249*(1), 126–137. https://doi.org/10.1006/jmbi.1995.0284

Misselwitz, B., Staeck, O., Matlack, K. E. S., & Rapoport, T. A. (1999). Interaction of BiP with the J-domain of the Sec63p Component of the Endoplasmic Reticulum Protein Translocation Complex. *Journal of Biological Chemistry*, *274*(29), Article 29. https://doi.org/10.1074/jbc.274.29.20110

Mori, H., & Cline, K. (2001). Post-translational protein translocation into thylakoids by the Sec and ΔpH-dependent pathways. *Biochimica et Biophysica Acta (BBA) - Molecular Cell*

Research, *1541*(1–2), 80–90. https://doi.org/10.1016/S0167-4889(01)00150-1

Nelson, M. K., Kurihara, T., & Silver, P. A. (1993). Extragenic suppressors of mutations in the cytoplasmic C terminus of SEC63 define five genes in Saccharomyces cerevisiae. *Genetics*, *134*(1), 159–173. https://doi.org/10.1093/genetics/134.1.159

Ng, D. T., Brown, J. D., & Walter, P. (1996). Signal sequences specify the targeting route to the endoplasmic reticulum membrane. *The Journal of Cell Biology*, *134*(2), Article 2. https://doi.org/10.1083/jcb.134.2.269

Palade, G. (1975). Intracellular Aspects of the Process of Protein Synthesis. *Science*, *189*(4200), 347–358. https://doi.org/10.1126/science.1096303

Park, E., & Rapoport, T. A. (2012). Mechanisms of Sec61/SecY-Mediated Protein Translocation Across Membranes. *Annual Review of Biophysics*, *41*(1), 21–40. https://doi.org/10.1146/annurev-biophys-050511-102312

Peña-Oyarzun, D., Rodriguez-Peña, M., Burgos-Bravo, F., Vergara, A., Kretschmar, C., Sotomayor-Flores, C., Ramirez-Sarmiento, C. A., De Smedt, H., Reyes, M., Perez, W., Torres, V. A., Morselli, E., Altamirano, F., Wilson, C. A. M., Hill, J. A., Lavandero, S., & Criollo, A. (2021). PKD2/polycystin-2 induces autophagy by forming a complex with BECN1. *Autophagy*, *17*(7), 1714–1728. https://doi.org/10.1080/15548627.2020.1782035

Pobre, K. F. R., Poet, G. J., & Hendershot, L. M. (2019). The endoplasmic reticulum (ER) chaperone BiP is a master regulator of ER functions: Getting by with a little help from ERdj friends. *Journal of Biological Chemistry*, *294*(6), Article 6. https://doi.org/10.1074/jbc.REV118.002804

Quiroga-Roger, D., Alfaro-Valdés, H. M., & Wilson, C. A. M. (2022). Posttranslational Protein Translocation through Membranes at the Single-Molecule Level. In K. Appasani & R. K. Appasani (Eds.), *Single-Molecule Science* (1st ed., pp. 80–94). Cambridge University

Press. https://doi.org/10.1017/9781108525909.010

Ramírez, M. P., Rivera, M., Quiroga-Roger, D., Bustamante, A., Vega, M., Baez, M., Puchner, E. M., & Wilson, C. A. M. (2017). Single molecule force spectroscopy reveals the effect of BiP chaperone on protein folding. *Protein Science*, *26*(7), 1404–1412. https://doi.org/10.1002/pro.3137

Rasband, W. S. (1997). *ImageJ* [Computer software]. U. S. National Institutes of Health.

Rico-Pasto, M., Alemany, A., & Ritort, F. (2022). Force-Dependent Folding Kinetics of Single Molecules with Multiple Intermediates and Pathways. *The Journal of Physical Chemistry Letters*, *13*(4), 1025–1032. https://doi.org/10.1021/acs.jpclett.1c03521

Rivera, M., Burgos-Bravo, F., Engelberger, F., Asor, R., Lagos-Espinoza, M. I. A., Figueroa, M., Kukura, P., Ramírez-Sarmiento, C. A., Baez, M., Smith, S. B., & Wilson, C. A. M. (2023). Effect of temperature and nucleotide on the binding of BiP chaperone to a protein substrate. *Protein Science*, *32*(7), Article 7. https://doi.org/10.1002/pro.4706

Rivera, M., Mjaavatten, A., Smith, S. B., Baez, M., & Wilson, C. A. M. (2023). Temperature dependent mechanical unfolding and refolding of a protein studied by thermo-regulated optical tweezers. *Biophysical Journal*, *122*(3), 513–521. https://doi.org/10.1016/j.bpj.2022.12.034

Robeson, L., Casanova-Morales, N., Burgos-Bravo, F., Alfaro-Valdés, H. M., Lesch, R., Ramírez-Álvarez, C., Valdivia-Delgado, M., Vega, M., Matute, R. A., Schekman, R., & Wilson, C. A. M. (2024). Characterization of the interaction between the Sec61 translocon complex and ppαF using optical tweezers. *Protein Science*, *33*(6). https://doi.org/10.1002/pro.4996

Rothblatt, J. A., Deshaies, R. J., Sanders, S. L., Daum, G., & Schekman, R. (1989). Multiple genes are required for proper insertion of secretory proteins into the endoplasmic reticulum in yeast. *The Journal of Cell Biology*, *109*(6), Article 6.

https://doi.org/10.1083/jcb.109.6.2641

Rukes, V., Rebeaud, M. E., Perrin, L. W., De Los Rios, P., & Cao, C. (2024). Single-molecule evidence of Entropic Pulling by Hsp70 chaperones. *Nature Communications*, *15*(1). https://doi.org/10.1038/s41467-024-52674-y

San Martín, Á., Rodriguez-Aliaga, P., Molina, J. A., Martin, A., Bustamante, C., & Baez, M. (2017). Knots can impair protein degradation by ATP-dependent proteases. *Proceedings of the National Academy of Sciences*, *114*(37), 9864–9869. https://doi.org/10.1073/pnas.1705916114

Sánchez, W. N., Driessen, A. J. M., & Wilson, C. A. M. (2025). Protein targeting to the ER membrane: Multiple pathways and shared machinery. *Critical Reviews in Biochemistry and Molecular Biology*, *60*(1–3), 33–79. https://doi.org/10.1080/10409238.2025.2503746

Sánchez, W. N., Robeson, L., Alfaro-Valdés, H. M., Tych, K., Matute, R. A., Driessen, A. J. M., & Wilson, C. A. M. (2026). Hydrophobicity and signal sequence binding to the Sec complex: A single molecule biophysical perspective. *Biochemical and Biophysical Research Communications*, *832*, 154361. https://doi.org/10.1016/j.bbrc.2026.154361

Sánchez, W. N., Robeson, L., Carrasco, V., Figueroa, N. L., Burgos-Bravo, F., Wilson, C. A. M., & Casanova-Morales, N. (2022). Determination of protein–protein interactions at the single-molecule level using optical tweezers. *Quarterly Reviews of Biophysics*, *55*, e8. https://doi.org/10.1017/S0033583522000075

Scidmore, M. A., Okamura, H. H., & Rose, M. D. (1993). Genetic interactions between KAR2 and SEC63, encoding eukaryotic homologues of DnaK and DnaJ in the endoplasmic reticulum. *Molecular Biology of the Cell*, *4*(11), 1145–1159. https://doi.org/10.1091/mbc.4.11.1145

Serway, R. A., Jewett, J. W., & Peroomian, Vahé. (2014). *Physics for scientists and engineers*

(Ninth edition). Cengage Brooks/Cole.

Shan, S. (2023). Role of Hsp70 in Post-Translational Protein Targeting: Tail-Anchored Membrane Proteins and Beyond. *International Journal of Molecular Sciences*, *24*(2), 1170. https://doi.org/10.3390/ijms24021170

Shao, S., & Hegde, R. S. (2011). A Calmodulin-Dependent Translocation Pathway for Small Secretory Proteins. *Cell*, *147*(7), 1576–1588. https://doi.org/10.1016/j.cell.2011.11.048

Smith, D. E., Tans, S. J., Smith, S. B., Grimes, S., Anderson, D. L., & Bustamante, C. (2001). The bacteriophage φ29 portal motor can package DNA against a large internal force. *Nature*, *413*(6857), 748–752. https://doi.org/10.1038/35099581

Stigler, J., & Rief, M. (2012). Calcium-dependent folding of single calmodulin molecules. *Proceedings of the National Academy of Sciences*, *109*(44), 17814–17819. https://doi.org/10.1073/pnas.1201801109

Stigler, J., Ziegler, F., Gieseke, A., Gebhardt, J. C. M., & Rief, M. (2011). The Complex Folding Network of Single Calmodulin Molecules. *Science*, *334*(6055), 512–516. https://doi.org/10.1126/science.1207598

Trombetta, E. S. (2003). The contribution of N-glycans and their processing in the endoplasmic reticulum to glycoprotein biosynthesis. *Glycobiology*, *13*(9), 77R – 91. https://doi.org/10.1093/glycob/cwg075

Tubiana, T., Carvaillo, J.-C., Boulard, Y., & Bressanelli, S. (2018). TTClust: A Versatile Molecular Simulation Trajectory Clustering Program with Graphical Summaries. *Journal of Chemical Information and Modeling*, *58*(11), 2178–2182. https://doi.org/10.1021/acs.jcim.8b00512

Van Holde, K. E., Johnson, W. C., & Ho, P. S. (2006). *Principles of physical biochemistry* (2. ed., internat. ed). Pearson/Prentice Hall.

Wang, X., Li, S., Wang, H., Shui, W., & Hu, J. (2017). Quantitative proteomics reveal proteins

enriched in tubular endoplasmic reticulum of Saccharomyces cerevisiae. *eLife*, *6*, e23816. https://doi.org/10.7554/eLife.23816

Waters, M. G., Evans, E. A., & Blobel, G. (1988). Prepro-alpha-factor has a cleavable signal sequence. *The Journal of Biological Chemistry*, *263*(13), 6209–6214.

West, M., Zurek, N., Hoenger, A., & Voeltz, G. K. (2011). A 3D analysis of yeast ER structure reveals how ER domains are organized by membrane curvature. *Journal of Cell Biology*, *193*(2), 333–346. https://doi.org/10.1083/jcb.201011039

Wilson, C. A. M. (2011). *Single molecule studies by optical tweezers: Folding and unfolding of glucokinase from Thermococcus litorali* [Universidad de Chile]. https://repositorio.uchile.cl/handle/2250/114149

Wilson, C. A. M., Alfaro-Valdés, H. M., Kaplan, M., & D'Alessio, C. (2025). Mechanical effect of protein glycosylation on BiP-mediated post-translational translocation and folding in the endoplasmic reticulum. *Biophysical Reviews*, *17*(2), 435–447. https://doi.org/10.1007/s12551-025-01313-x

Wu, X., Cabanos, C., & Rapoport, T. A. (2019). Structure of the post-translational protein translocation machinery of the ER membrane. *Nature*, *566*(7742), Article 7742. https://doi.org/10.1038/s41586-018-0856-x

Yamano, K., Kuroyanagi-Hasegawa, M., Esaki, M., Yokota, M., & Endo, T. (2008). Step-size analyses of the mitochondrial Hsp70 import motor reveal the Brownian ratchet in operation. *The Journal of Biological Chemistry*, *283*(40), 27325–27332. https://doi.org/10.1074/jbc.M805249200

Zhang, M., Tanaka, T., & Ikura, M. (1995). Calcium-induced conformational transition revealed by the solution structure of apo calmodulin. *Nature Structural & Molecular Biology*, *2*(9), 758–767. https://doi.org/10.1038/nsb0995-758

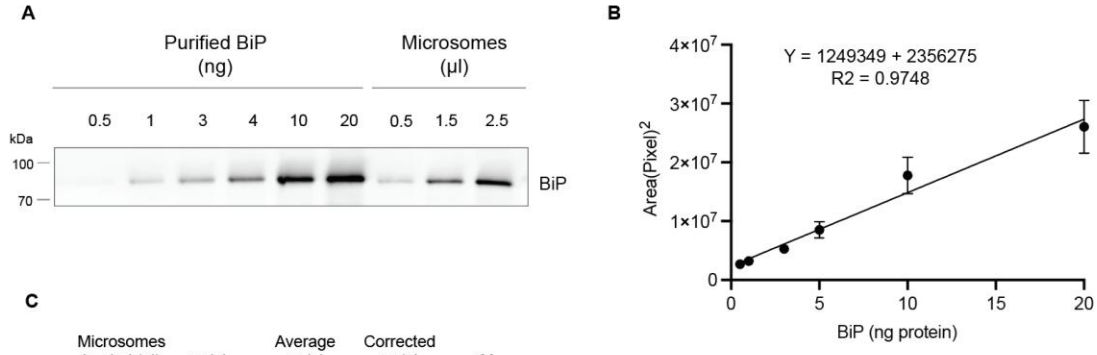
Zimmermann, R., Eyrisch, S., Ahmad, M., & Helms, V. (2011). Protein translocation across the

ER membrane. *Biochimica et Biophysica Acta (BBA) - Biomembranes*, *1808*(3), 912–924. https://doi.org/10.1016/j.bbamem.2010.06.015

Zimmermann, R., & Lang, S. (2020). A Little AXER ABC: ATP, BiP, and Calcium Form a Triumvirate Orchestrating Energy Homeostasis of the Endoplasmic Reticulum. *Contact*, *3*, 251525642092679. https://doi.org/10.1177/2515256420926795

APPENDIX A

Supplemental Material



C

Microsomes loaded (µl)	ng/µl	Average ng/µl	Corrected ng/µl	µM
0.5	1.89	2.67	513.27	6.88
1.5	2.87			
2.5	3.25			

Figure S1. Estimation of BiP concentration in microsomes. **(A)** Semi-quantitative immunoblot analysis to estimate the concentration of BiP in microsomes. Increasing volumes of diluted microsomes, as well as increasing ng of purified and wild-type BiP, were separated by SDS-PAGE and analyzed by Western blotting using anti-BiP (1:10,000). **(B)** The purified BiP bands were densitometrically scanned, and values were plotted against the different amounts of loaded BiP. **(C)** We estimated BiP concentration in microsomes using the equation from the linear regression in B and corrected for the corresponding dilution factors (see Materials and Methods). In B, data are expressed as the mean ± SEM (N=2 independent experiments).

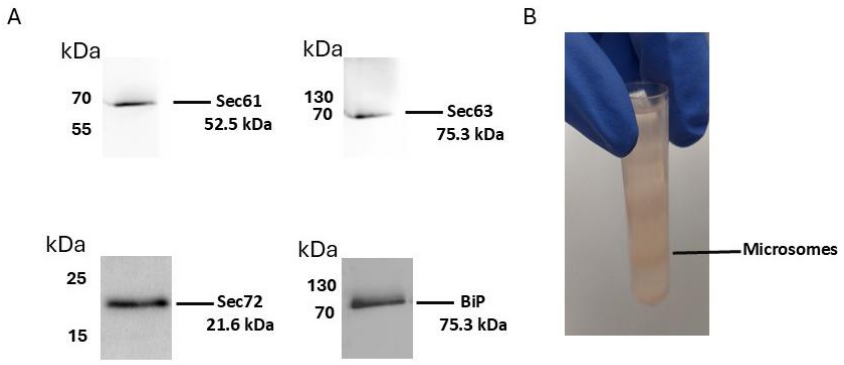


Figure S2. Components of the Sec61 translocon from microsomes of the RSY1255 yeast strain. (A) Western blot analysis of isolated microsomes from the RSY1255 strain showing the translocon core and accessory components anti-Sec61 (1:5,000), anti-Sec63 (1:10,000), anti-Sec72 (1:500), and anti-BiP (1:10,000). **(B)** Isolation of the microsomal fraction via density gradient ultracentrifugation, showing the distinctive microsome band at the interface between the 1.2 M and 1.5 M sucrose layers.

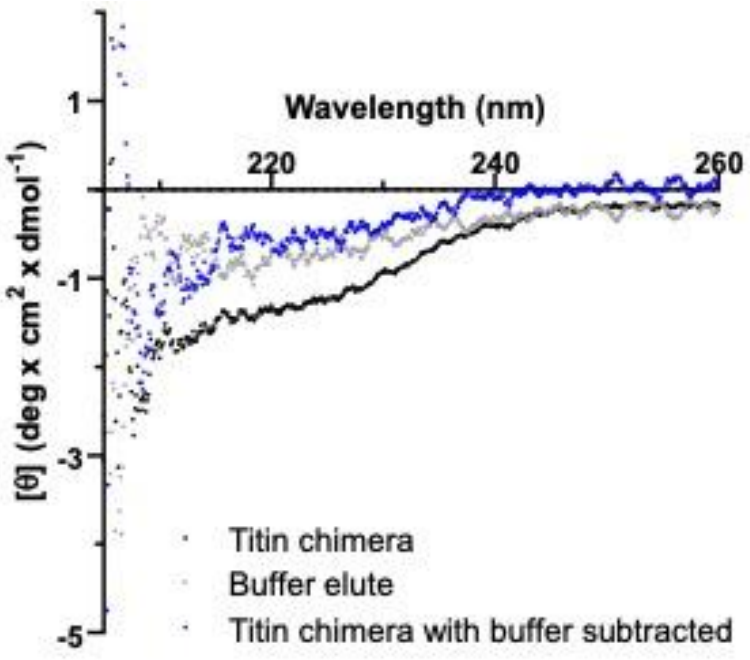


Figure S3. Circular dichroism spectra of the double unfolded Titin I27 mutant chimera. Mean Residue Ellipticity (MRE) spectrum showing a random coil/denatured profile without the characteristic 220 nm minimum of native β-sheets or the 208 nm and 222 nm minima characteristic of α-helix, confirming an unstructured state for translocation for the Titin I27 mutant chimera (in blue with buffer subtracted).

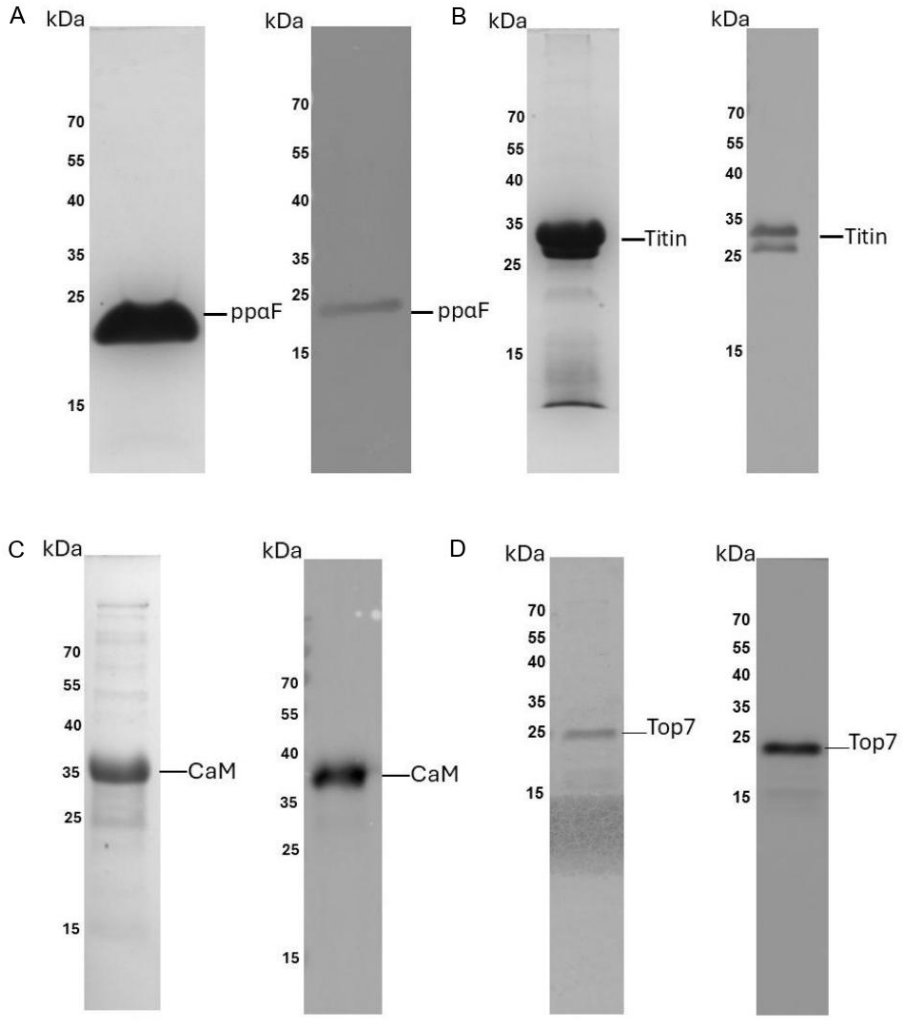


Figure S4. Purification of proteins for Translocation Assays. Purified His-tagged ppαF and chimera proteins were visualized by Coomassie staining (left) and Western blot with a specific antibody to each protein or against His-tag (right). **(A)** PpαF at 19 kDa, **(B)** Titin at 28 kDa, **(C)** CaM at 35 kDa, and **(D)** Top7 at 24.5 kDa. All proteins showed the expected size in both visualization methods.

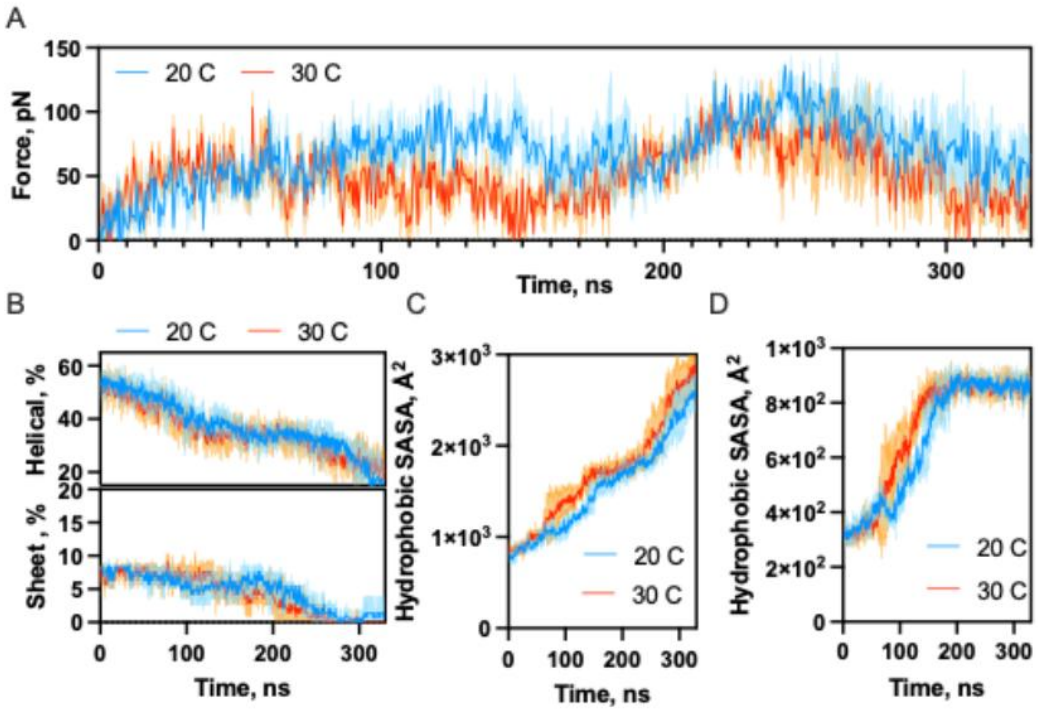


Figure S5. Apo-Calmodulin pulling at different temperatures in steered molecular dynamics. We performed six replicates of 330 ns of pulling molecular dynamics (SMD) at 0.04 nm/ns for apo CaM at different temperatures. **(A)** Force evolution throughout the pulling simulation at 20 °C and 30 °C. The force dependency curves are almost superimposable except for the region of unfolding between 100-200 ns, where the N-terminal helix of CaM unfolds. Secondary structure content of the whole protein throughout the simulations. **(B)** and hydrophobic residue exposure to solvent for the Whole protein in **(C)** or the helix H1 only in **(D)**. In these plots, hydrophobic exposure of apo CaM at 30 °C occurs ~50 ns more rapidly than at 20 °C. All curves are plotted as mean ± SD.

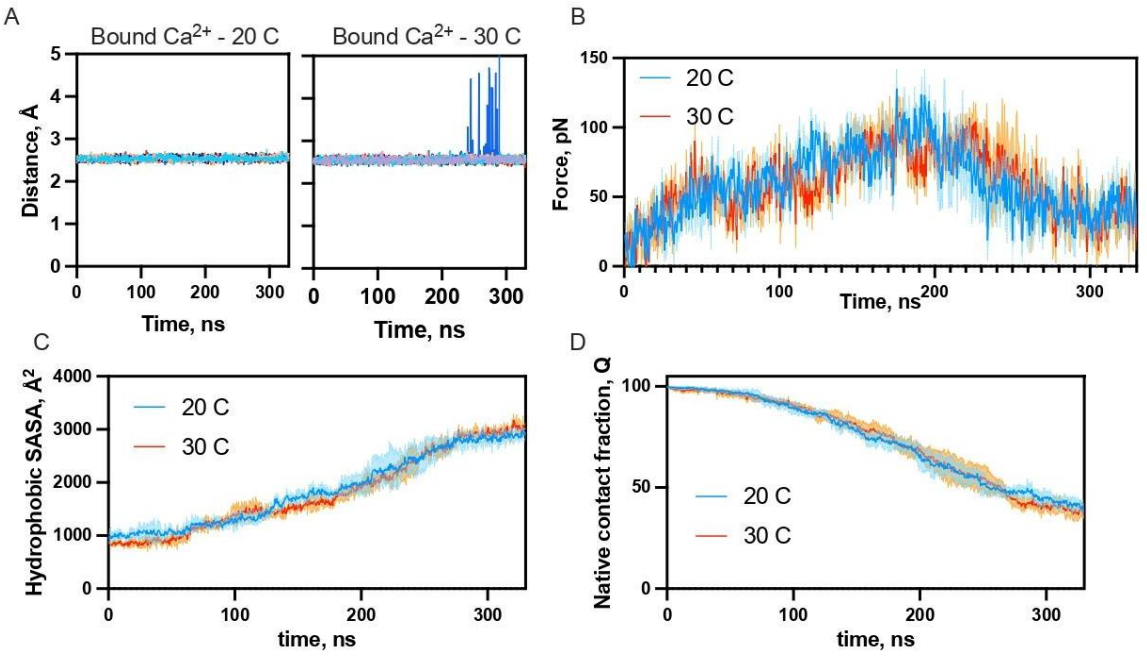


Figure S6. Steered molecular dynamics (SMD) unfolding of the Ca^{2+}-bound Holo-calmodulin N-lobe EF-hand domain at 20 °C and 30 °C. The N-terminal CA was harmonically restrained as a fixed anchor, and the C-terminal CA was pulled at a constant rate of 0.04 nm/ns with six independent replicates per temperature, same as for apo CaM. **(A)** Distance from each bound Ca^{2+} ion to its nearest native coordinating oxygen from the EF-hand loop, shown for all six replicates. Ca^{2+} coordination remains at its native distance (~2.5 Å) throughout the pull in nearly every replicate. Only one 30 °C replicate shows a single dissociation event after most structure is unfolded. **(B)** Pulling force on the C-terminal restraint versus time (mean ± SEM, n = 6 per temperature). The traces are almost identical between temperatures. **(C)** Solvent-accessible surface area (SASA) of hydrophobic side chains (mean ± SD, n = 6). Here, side-chain exposure in holo CaM no longer differs from apo. **(D)** Fraction of native CA–CA contacts retained (Q), defined using an 8 Å native-contact cutoff with 1.2 times the native distance tolerance relative to each replica's starting structure (mean ± SD, n = 6). Native contact reduction is nearly monotonic throughout the simulations, with a significant portion (~40%) remaining after global unfolding due to the Ca^{2+} site-holding force.

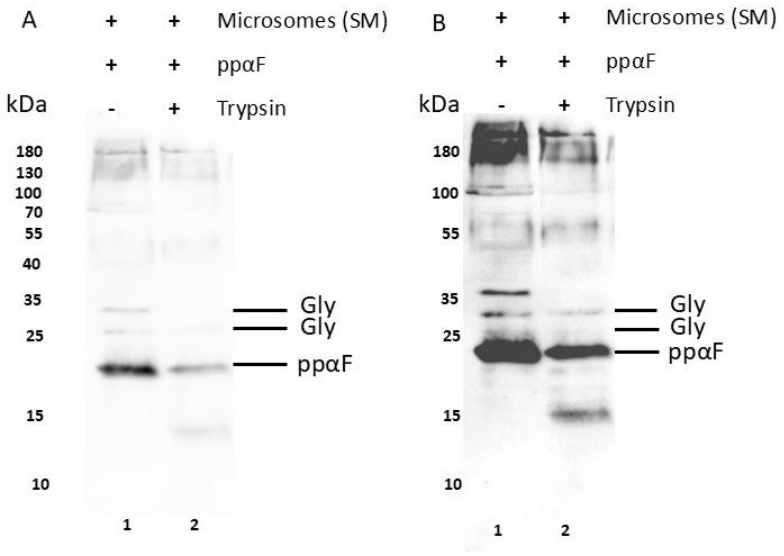


Figure S7. Microsomal functionality verified by *in vitro* translocation and glycosylation. Western blot analysis using labelled ppαF. Functional microsomes are demonstrated in lanes 4 and 5 by the appearance of slower-migrating glycosylated bands (Gly), which occur only after successful translocation into the microsomal lumen. The partial protection of these Gly bands against Trypsin digestion (lane 5 vs 4) further confirms that ppαF was internalized and modified within intact microsomal membranes.

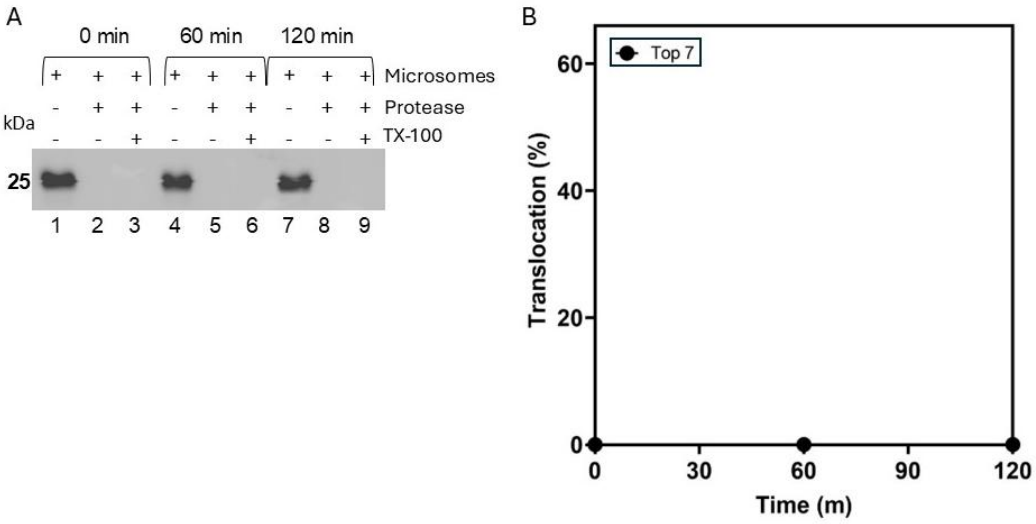


Figure S8. Translocation assay of Top7 into microsomes. (A) Western blot analysis of Top7 (~25 kDa) incubated with microsomes over time (0, 60, and 120 min). Upon protease addition (lanes 2, 5, and 8), Top7 is completely degraded at all time points, regardless of Triton X-100 (TX-100) addition, indicating a lack of protease protection and failure to translocate into the microsomal lumen. **(B)** Quantification of Top7 translocation efficiency over time, showing 0% translocation at all tested time points.

Sequence of chimeric proteins

Titin I27 mutant chimera

MRFPSIFTAVLFAASSALAGGGHMGSEFGGGGGSLIEVEKPLYGVEPFPG
ETAHFEIELSEPDVHGQWKLKGQPLAASPDEEIIEDGKKHILILHNEQL
GMTGEVSFQAANTKSAANLKVKEFLGSGGMEFLIEVEKPLYGVEPFPGET
AHFEIELSEPDVHGQWKLKGQPLAASPDEEIIEDGKKHILILHNEQLGMT
GEVSFQAANTKSAANLKVKESRHHHHHH

Figure S9. Amino acid sequence and domain organization of the chimeric Titin I27 mutant construct (227 amino acids). Primary sequence of the engineered protein chimera Titin I27 mutant chimera. Distinct structural regions and functional motifs are annotated as follows: the N-terminal signal sequence (residues 1–19, *yelow*), flanking and intermediate flexible linkers (residues 20–34 and 123–131, 220-221 *Magenta*), sequence of Titin I27 mutant (residues 35–122, *grew*), sequence of Titin I27 mutant (residues 132–219, *grew*), and the C-terminal 6×His-tag (residues 222–227, *Red*). Theoretical molecular weight (M_w) and isoelectric point (pI) were computed using the ExPASy Compute pI/Mw tool 5.31 and 24.62 kDa.

CaM chimera

MRFPSIFTAVLFAASSALAGGGHMGSEFGGGGGSLIEVEKPLYGVEPFPG
ETAHFEIELSEPDVHGQWKLKGQPLAASPDEEIIEDGKKHILILHNEQLGM
TGEVSFQAANTKSAANLKVKEFLGSGGMEFADQLTEEQIAEFKEAFSLFD
KDGDGTITTKELGTVMRSLGQNPTEAELQDMINEVDADGNGTIDFPEFLT
MMARKMKDTDSEEEIREAFRVFDKDGNGYISAAELRHVMTNLGEKLTDE
EVDEMIREADIDGDGQVNYEEFVQMMTAKSRHHHHHH

Figure S10. Amino acid sequence and domain organization of the chimeric CaM construct (287 amino acids). Primary sequence of the engineered protein chimera CaM. Individual domains and structural motifs are color-coded and annotated as follows: the N-terminal signal sequence (residues 1–19, *yellow*), linkers (residues 20–34, 123–131, 280-281 *Magenta*), the Titin I27 mutant domain (residues 35–122), sequence of Calmodulin protein (residues 132–279, *Blue*), and C-terminal 6×His-tag (residues 282–287, *Red*). Theoretical molecular weight (M_w) and isoelectric point (pI) were computed using the ExPASy Compute pI/Mw tool 4.56 and 31.6 kDa.

Top7 chimera

MGFPSIFTAVLFAASSALAGGGHMGSEFGGGGGSLIEVEKPLYGVEPFP
GETAHFEIELSEPDVHGQWKLKGQPLAASPDEEIIEDGKKHILILHNEQL
GMTGEVSFQAANTKSAANLKVKEFLGSGGMEFDIQVQVNIDDNGKNFD
YTYTVTTESELQKVLNELKDYIKKQGAKRVRISITARTKKEAEKFAAILIKV
FAELGYNDINVTFDGDTVTVEGQLESRHHHHHH

Figure S13. Amino acid sequence and domain organization of the chimeric Top7 construct (232 amino acids). Primary sequence of the engineered protein chimera Top7. Functional segments and structural domains are annotated as follows: the N-terminal signal sequence (residues 1–19, *yelow*), flanking and intermediate flexible linkers (residues 20–34 and 123–130, 225-226 *magenta*), the Titin I27 mutant domain (residues 35–122), Top7 sequence protein (residues 131–224, *green*), and the C-terminal 6 × His-tag (residues 227–232, *Red*). Theoretical molecular weight (M_w) and isoelectric point (pI) were computed using the ExPASy Compute pI/Mw tool 5.44 and 25.24 kDa.

Comparison	20°C	30°C
Titin vs CaM	0.0008***	< 0.0001****
Titin vs CaM + EGTA	< 0.0001****	0.0001***
Titin vs Top7	< 0.0001****	< 0.0001****
CaM vs CaM + EGTA	0.8859	0.008**
Top7 vs CaM	0.0276*	0.1425
Top7 vs CaM + EGTA	0.0043**	0.0007***

Table S1. p-values of t-tests comparing chimera maximum translocation values at 20°C and 30°C. Maximum (after 2 hours) levels of translocation measured for each chimera at 20°C and 30°C. T-tests performed to compare outcomes of different chimera studies at given temperatures and p-values reported here (* $p < 0.05$, ** $p < 0.01$, *** $p < 0.001$, **** $p < 0.0001$).

Reagent	Brand	Catalog number
Acrylamide	Invitrogen	15512023
Agar-Agar	Merck	1016141000
Agarose	Merck	16802
Ampicillin sodium salt	Sigma	A0166
Sodium azide	Sigma	S2002
BamHI	New England BioLabs	R0136S
EasyTag Methionine L-[36S]	PerkinElmer	NEG709A500UC
EcoRI	New England BioLabs	R01015
E-64	Sigma	1002110975
0.5 mm Zirconia/Silica beads	BioSpec	11079105z
Yeast extract	winkler	212750
Phenylmethylsulfonyl fluoride	Sigma	78830-1G
Glycine	Merck	120081000
D-Glucose	Merck	1083421000
HindIII	New England BioLabs	R01045
Imidazol	UsBiological	288-32-4
Isopropyl β-D-1-thiogalactopyranoside	Gold-Bio	12481C25
Leupeptine	Sigma	L0649-5MG
Nitrocelullose Membrane	Macherey-Nagel	741280
Methanol	Merck	1.06009.2500
Sodium Chloride	New England BioLabs	R0193S
NcoI	New England BioLabs	R0111S
NdeI	Sigma	P5318
Pepstatine	Merck	72161000
Peptone	Merck	7651
Sacarose	Life Technologies	EP0402
Yeast nitrogen base without amino acids	Sigma	Y0626-250G
Drop-out Mix Synthetic Minus Uracil w/o Yeast Nitrogen Base (Powder)	US Biological Life Sciences	L1910408
Drop-out Mix Synthetic Minus Leucine w/o Yeast Nitrogen Base (DO, Dropout, Broth)	US Biological Life Sciences	L2303
Taq DNA polimerase	New England BioLabs	M0202S
5-Fluoroorotic acid	Sigma	F-5013

Table S2. Reagents used in this thesis.

APPENDIX B

Response to Reviewer Comments

In this Appendix, we present the response letter regarding the review of the manuscript "The Endoplasmic Reticulum master regulator protein BiP acts as a ratchet molecular motor in translocation" by Hilda M. Alfaro-Valdés et al., submitted to the Proceedings of the National Academy of Sciences (PNAS) journal.

Response letter

We thank the reviewer for their comments, which we believe have improved our paper. In this response letter, the comments appear in bold face, and our answers are in regular font. In the new version, we have included all changes and suggestions.

Comments

1. **Fig. S1: CaM is not really purified, as the Coomassie-stained SDS-gel shows many bands larger and smaller than 35 kDa. Purity is certainly less than 50%. To judge the purity of the Top7 chimera, the authors need to load at least 10-fold higher amounts.**

We thank the reviewer for the constructive feedback regarding protein purity and characterization. We performed a new purification of the Calmodulin (CaM) construct using an optimized protocol. The updated SDS-PAGE in **Figure S3** shows a markedly improved purity profile. However, bands previously observed by mass spectrometry (MS) in CaM showed greater impurity, corroborating that the signal sequence is present in the

constructs (such as our Titin control, displaying 28 kDa and 25 kDa species), and confirming that lower-molecular-weight bands represent truncated species lacking the signal sequence.

Therefore, in the protease protection assay, the unfolded Titin I27 mutant chimera construct selectively protected only the full-length, signal-containing protein (28 kDa) and eliminated the 25 kDa band, demonstrating that non-functional truncated forms do not interfere with the translocation machinery.

Furthermore, a functional translocation assay using the new purified CaM showed a normalized translocation efficiency of 9.2% at 60 minutes, which aligns fully with our established historical range under identical conditions (5.1%–16.2%, mean ~11.7%).

2. **Fig. S2: panel A: in the absence of microsomes a fraction of the titin chimera seems protected from protease digestion. This fraction is obviously sensitive to Triton X-100. When comparing lane 1 and 2 of panel A (absence of microsomes) with lane 1 and 2 of panel C (presence of microsomes and ATP) the degree of protection appears very similar. These results question the validity of the translocation assay. Furthermore, the authors should detect in addition BiP, which should be completely protected from degradation in the absence of Triton X-100, and an ER surface marker, which should be degraded in the presence of the protease. These bands could be used for normalization.**

Thanks for pointing this out. When our assays were performed without an optimized protocol, we performed an assay in the absence of microsomes to corroborate protein aggregation of the unfolded Titin I 27 mutant chimera. As an unfolded protein, Titin tends to aggregate over time. In these conditions, the protein aggregates over time. We observed that this effect was substantially reduced in the presence of microsomes, concluding that

the membranes improve the digestion of the protein. However, aggregation occurs after a long incubation period and can still be observed, for example, at 120 min (**Figure 11**).

To improve visual clarity regarding the protection controls (PK + TX-100), we optimized the protocol by adding Triton X-100 during the final 10 minutes of the 30-minute protease incubation on ice, ensuring efficient solubilization of the membranes and complete digestion and protection of protein by microsomes. We obtained a clean and improved result in this assay (PK + Triton X-100) at 30 °C. With yielding a normalized protection level of 44.6% at 1 hour (presented in the new Supplementary **Figure R7**). This value aligns fully with our established experimental range and historical thesis dataset under identical conditions (30 °C), confirming both the reproducibility of our microsomal transport system and that the protected bands correspond strictly to fully translocated, membrane-enclosed proteins rather than non-specific aggregation artifacts.

Finally, non-translocator controls, such as the folded Top7 protein, do not exhibit any protected band under these conditions, confirming that the protection observed in the presence of microsomes is not a non-specific aggregation artifact or an intrinsic resistance to proteases (**Figure S6**), but rather represents true membrane-bound luminal translocators that are completely degraded when the membrane solubilizes, as they are not fully unfolded.

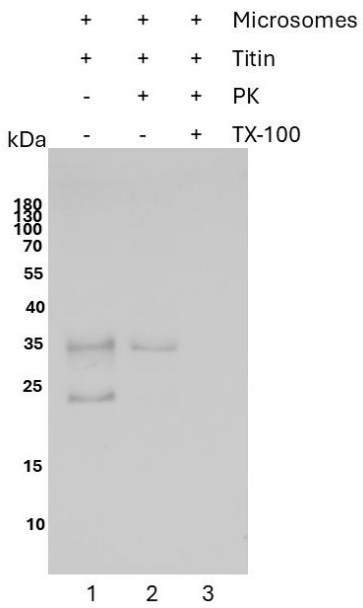


Figure R7. Optimized protease protection assay of Titin chimera at 30 °C. Western blot analysis demonstrates luminal translocation efficiency of the Titin chimera under optimized solubilization conditions. Lane 1, total input. Lane 2 demonstrates specific protection of the full-length 28 kDa translocated protein against Proteinase K (PK) digestion. Lane 3 confirms complete substrate degradation with improved membrane solubilization using Triton X-100 (TX, added during the final 10 min of digestion), indicating the absence of non-specific aggregation or false-positive protease resistance.

3. **Fig. S4: the protection of the CaM construct is really hard to see. The authors should leave an empty lane between the load and the trypsin treated sample. Again, even in the absence of microsomes some protection from degradation is observed and this protection is more prominent than in the presence of microsomes.**

We would like to clarify a display error in the previous version of **Figure S4.** The corresponding panels have now been updated with the correct representative curves/data used to calculate the translocation rates. Additionally, to ensure a direct and consistent comparison with the other experimental conditions (rates), the analysis was standardly truncated/restricted to a 60-minute timeframe as shown in **Figure R8**.

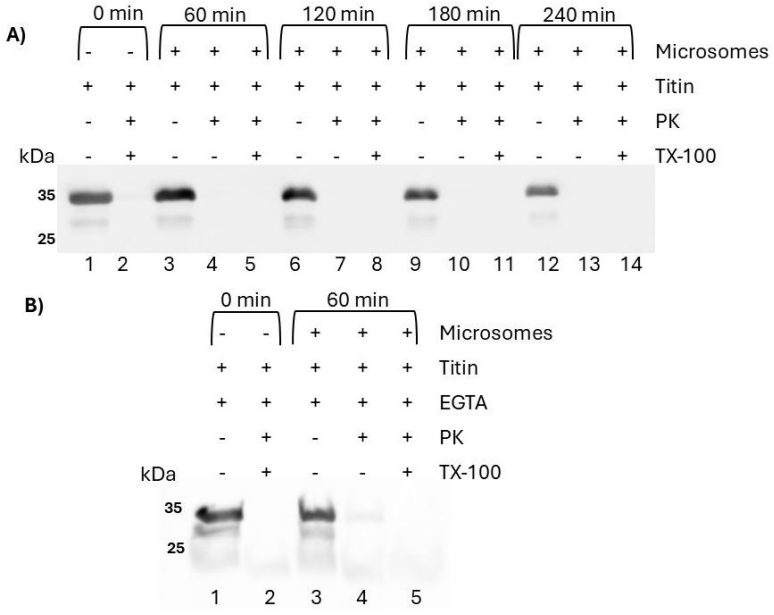


Figure R8. Kinetic evaluation of CaM chimera translocation at 20°C vs 30°C and EGTA. A) Time-course translocation assay of CaM chimera up to 240 min at 20°C. For each point, conditions represent total input (left lane), Proteinase K (PK) protection (middle lane), and solubilization control (+PK +TX-100, right lane). The complete absence of signal in all TX-100 solubilization lanes (lanes 5, 8, 11, and 14) confirms that restricting Triton X-100 to digestion prevents hydrophobic aggregation artifacts over extended incubation times. **B)** Translocation protection assay of CaM chimera at 60 min in the presence of EGTA at 30°C. Showing specific luminal protection of the 35 kDa species in lane 4 and total clearance upon membrane disruption in lane 5, as reported in Section 3.4 and Table 1 of this work.

4. **The authors state that the protein levels of the protected band decreases after 3 and 4 h. How can this be? Actually, the protein band in the absence of trypsin also decreases with time, indicating that the CaM construct or the microsomes or both are contaminated with proteases. As the "purified" CaM construct showed a large number of additional bands this is not surprising. Under these conditions the values derived from such a construct are not reliable. Furthermore, in the lower panel the CaM band in the presence of Triton X-100 is as intense as the band in the absence of Triton X-100 indicating that aggregation is also a problem with this construct.**

We thank the reviewer for raising these points regarding the CaM construct controls and time-course behavior. As clarified in our response to the previous comment regarding the display error in the former gel panels, our CaM construct was consistently sound and functional throughout. The minor signal persistence previously observed in the absence of microsomes was simply due to a slight, intrinsic tendency of the substrate to form minor hydrophobic aggregates in bulk solution. Crucially, in the presence of microsomes, this aggregation is completely abolished, allowing complete degradation of non-translocated CaM.

5. **Fig. 3: panel A: the authors should show the radioactive assay (lanes 3 - 5) also in the absence of microsomes; when comparing lane 3 and 4 it becomes apparent that the bands the authors indicated as glycosylated pαF is diminished in the presence of protease. How could that be as glycosylation is considered to be an indication of translocation into the ER? Panel B: the authors designated a band at 35 kDa as glycosylated pro-α-factor (gpαF). Why is such a band visible in lane 1 from a reaction that did not contain microsomes? In contrast, very little ppαF is detected in lane 1, presumably because it is aggregated under the conditions of the experiment. The fact that a fraction of the ppαF is not degraded in the presence of detergent makes quantification even more difficult.**

We appreciate the opportunity to clarify the labeling of the previous version in Figure 3. The high molecular weight band (~35 kDa) visible in lane 1 (in the absence of microsomes) does not reflect glycosylation, since N-glycosylation strictly requires that ppαF has translocated through the luminal machinery of functional ER microsomes.

In contrast, in immunoblotting, these bands correspond to a non-specific signal from the anti-ppαF antibody. To address this, we improved the detection signal by using the more diluted antibody (from 1:5000 to 1:10000), as shown in **Figure 10B**. Furthermore, we

resolved the aggregation using the optimized PK and TX-100 cutting protocol, eliminating the aggregation, as shown in our new **Figure 10B**, **lane 2**. It is worth noting that the translocation percentage obtained was like that of the radioactive film, although glycosylation was not quantified. This confirms that ppαF levels are similar in both cases. Furthermore, the quantified glycosylation contributes approximately 50% of what is reported in the literature when only the non-glycosylated band is quantified. Therefore, our protected protein levels fall within the expected range for ppαF (Brodsky et al., 1995; Lyman & Schekman, 1995). The important thing is that we observe the glycosylation as in **Figure S4** and started from this baseline quantification in our ppαF translocation assays to demonstrate its functionality. Furthermore, our chimera does not have glycosylation sites. Therefore, this assay was only performed to validate that our experimental model is viable for quantifying the translocation rates of the chemical proteins used in this work.

6. **Fig. 4A upper panel: the 35 kDa band in lane 9 is more intense than in lane 8. The authors explain the band in lane 9 as aggregated titin chimera. If this is not degraded in the presence of protease and detergent there is no evidence that the amount of titin chimera visible in the 35 kDa band in lane 8 is actually translocated titin chimera.**

Thank you for pointing this out. We agree with the reviewer that, in the previous version of the gel, the persistence of the signal in the solubilization control lane (+PK +TX-100) created ambiguity between true luminal protection and nonspecific substrate aggregation.

As detailed in our response to Comment 2, this artifact originated in our previous solubilization protocol, in which prolonged incubation with Triton X-100 and proteinase K promoted hydrophobic aggregation of the unfolded Titin chimera, preventing its complete cleavage. We resolved this technical limitation by optimizing the digestion protocol, restricting the use of Triton X-100 (0.3%) exclusively to the last 10 minutes of the 30-minute incubation with proteinase K on ice. This is shown in our updated representative gels (**Figure R7** and **Figure 11A**).

Membrane disruption under these conditions results in complete substrate digestion, with no residual band in the solubilization control lane. This unequivocally confirms that the 35 kDa protected band observed in the presence of intact microsomes (+PK, -TX-100) corresponds to true, membrane-bound luminal translocations, rather than nonspecific aggregation.

7. **Fig. 4D The use of the 120 min value is not appropriate as it cannot be distinguished which fraction of the titin chimera aggregated after translocation inside the microsomes and which fraction aggregated outside the microsomes before translocation.**

We appreciate the reviewer's comment regarding the reliability of extended time points. With our optimized solubilization protocol, we successfully eliminated the non-specific aggregation artifacts previously observed, ensuring robust quantification.

Specifically, restricting Triton, the complete clearance in the solubilization control lanes (+PK +TX-100) confirms that no detergent-resistant aggregates persist in interfering with proteolysis. Because the assay functions cleanly within this established regime, the protection observed at 120 minutes represents true luminal accumulation rather than external aggregation. However, to ensure maximum accuracy and comparability across all experimental conditions, our primary rate calculations and comparative analyses rely on the initial linear range (up to 60 minutes).

8. **How the authors arrive at an estimated 50 to 60% translocation after 120 min is also beyond me. The band intensity in the protease treated sample is certainly less than 10% of the band in the untreated sample. In Table S1 the authors indicate that translocation levels for titin chimera to be 14.5% in the absence of microsomes and ATP, 13% in the presence of microsomes and absence of ATP, and 21.2% in the presence of microsomes and ATP. This**

means the true translocation within 60 min at 20°C is 8.2%. Deriving from these data a translocation rate of 0.42%/min is not traceable for me. In my calculation this would be 0.14% per min. Even if the estimated translocation rate of 0.42%/min were correct, it would mean that the translocation of a 100-residues unfolded protein would take 240 min which is not meaningful for an organism that divides every 90 min; a rate of 0.14%/min would mean that complete translocation of a 100-residue unfolded protein would take >12h.

We thank the reviewer for raising these important points regarding our quantification and kinetic analysis. Below, we clarify the mathematical treatment, normalization, and derivation of the translocation rates.

With our optimized solubilization protocol, we successfully eliminated the previously observed nonspecific aggregation artifacts, ensuring robust quantification. Specifically, the Triton restriction and complete elimination in the solubilization control samples (+PK +TX-100) confirm that no detergent-resistant aggregates persist in interfering with proteolysis.

The values cited by the reviewer originated from a preliminary version of Table S1 containing raw, uncorrected densitometric values. In the final analysis, we background-corrected signals using the non-specific baseline at t = 0 for each condition, and calculated translocation as the protected band intensity relative to the total input substrate. Using this standardized normalization, the fully unfolded Titin chimera (0 pN positive control) reached (38.35 ± 10.44)% at 20 °C and (61.77 ± 4.01)% at 30 °C after 60 min (Table 2 and Figure 12). These values are consistent with the historical range of 40–66% reported for cell-free *S. cerevisiae* microsomal systems using classical substrates such as ppαF (Brodsky et al., 1993; Rothblatt et al., 1989).

In standard *in vitro* post-translational translocation assays using *S. cerevisiae* microsomes, the historically reported maximum translocation efficiency for unfolded reference

substrates (such as ppαF) ranges from 40% to 66%.

Under our optimized conditions, the fully unfolded titin chimera consistently produces a normalized protected fraction of ~30%–33% at 60 min (44.6% at 1 h, 30 °C). These values fall within the reference range established in the literature, confirming that our reconstituted microsomal machinery operates at full physiological capacity in an *in vitro* system.

We agree with the reviewer that a bulk population rate of 0.6-1.0% cannot be directly interpreted as the time required for a single 100-residue polypeptide to traverse an individual Sec61 channel. Such a calculation assumes that all substrate molecules and microsomal translocons are simultaneously and continuously competent for translocation. In bulk microsomal assays, however, vesicle heterogeneity, the fraction of transport-competent translocons, and limited luminal BiP availability contribute to the observed macroscopic rate. As quantified in Figure S1, luminal BiP concentration in our microsomes was 7-14 μM, substantially below physiological ER levels. Accounting for these factors, we estimate a microscopic translocation velocity of 1 nm/s (Section 3.6), consistent with previously reported (Liebermeister et al., 2001).

The primary purpose of this reconstituted *in vitro* assay is not to reproduce the rapid kinetics of *in vivo* protein translocation, but to provide a calibrated comparative framework for assessing the effect of substrate mechanical stability. Under identical microsomal conditions, the unfolded Titin chimera (0 pN) translocated efficiently at 0.61 %/min, whereas the 7 pN unfolded force of the CaM chimera showed strongly reduced translocation (0.03 %min), and the 20 pN unfolded force of the Top7 chimera showed no detectable translocation. Thus, increasing substrate mechanical stability markedly impairs translocation under otherwise identical conditions, supporting a model in which substrate unfolding and mechanical resistance strongly influence translocation efficiency, consistent with a passive Brownian-ratchet mechanism.

9. **In my opinion it is doubtful that the translocation assay actually worked as some protection for the titin chimera was even observed in the absence of microsomes as shown in Fig. S2 (as mentioned above). The observed protection might be aggregation of titin that is detergent sensitive during the first 60 min of incubation and then becomes detergent insensitive over time.**

We appreciate the reviewer's critical evaluation of the translocation assay's validity. We understand the concern that nonspecific substrate aggregation could be misinterpreted as luminal protection. However, multiple experimental studies unequivocally confirm that our assay measures actual translocation within the membrane, not aggregation artifacts. The residual band signal, in the absence of microsomes or after prolonged incubations with detergent and PK or Tryp in earlier gel versions, was due to our initial solubilization protocol. Prolonged incubation with the nonionic detergent (Triton X-100) of the unfolded titin chimera promoted aggregation of the hydrophobic substrate and physically protected the protease cleavage sites.

By refining the protocol, restricting the use of Triton X-100 exclusively to the last 10 minutes of the 30-minute incubation with Proteinase K, we achieved rapid and complete membrane solubilization without detergent-induced substrate aggregation. As demonstrated in our updated representative gels (**Figure R7** and **Figure 11A**), complete elimination (100% digestion) was obtained in the +PK +TX-100 lanes, indicating that no detergent-resistant aggregates persist in our system.

To rigorously rule out the possibility that the protected band represents non-specific aggregation or intrinsic protease resistance, we evaluated the Top7 chimera as a negative control. Top7 is a stably folded structure (with an unfolding force of approximately 20 pN) that interacts with the translocon but cannot translocate to the microsomes. As shown in Figure S6, Top7 exhibits 0% protection in the presence of microsomes and protease (+PK, -TX-100) at all time points. If the protection observed for the titin chimera were a

nonspecific aggregation artifact, Top7 would also exhibit protected bands. The complete lack of protection for Top7 confirms that the 35 kDa band of protected titin strictly requires successful translocation into the microsomal lumen.

Furthermore, mass spectrometry and Western blot analysis confirmed that only the complete protein containing the intact signal sequence (28–35 kDa) is selectively protected within microsomes, while truncated fragments lacking the signal sequence (e.g., 25 kDa) are completely degraded by the protease. This further underscores the biological and functional specificity of the translocation process in our system. Taken together, these controls demonstrate that the protease protection assay is fully functional, highly specific, and robustly distinguishes true luminal import from nonspecific aggregation.